

Refined modeling and co-optimization of electric-hydrogen-thermal-gas integrated energy system with hybrid energy storage

Haoxin Dong ^{a,b,*}, Zijing Shan ^{a,b}, Jianli Zhou ^c, Chuanbo Xu ^{a,b}, Wenjun Chen ^{a,b}

^a School of Economics and Management, North China Electric Power University, Beijing 102206, China

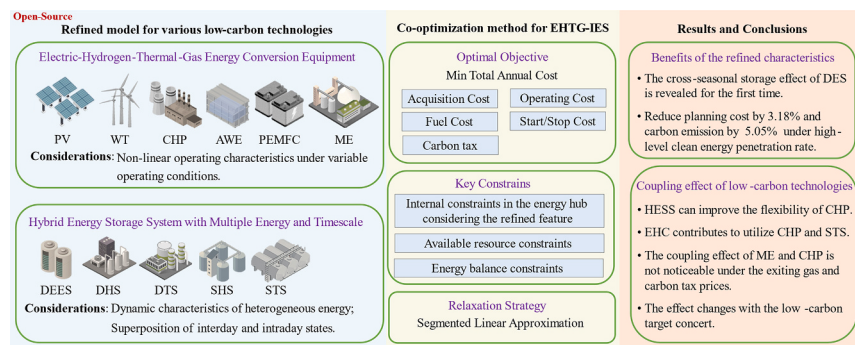
^b Beijing Key Laboratory of New Energy and Low-Carbon Development, North China Electric Power University, Changping, Beijing 102206, China

^c School of Economics and Management, Xinjiang University, Urumqi 830046, China

HIGHLIGHTS

- Various low-carbon technologies are finely modeled considering non-linear features.
- Linear-reduction and relaxation strategies are developed for hybrid energy storage.
- The complementary potential of low-carbon technologies is utilized and explained.
- Cost and CO₂ emissions are reduced thanks to the refined model for the system.

GRAPHICAL ABSTRACT



ARTICLE INFO

Keywords:
 Integrated energy systems
 Co-optimization
 Hybrid energy storage
 Hydrogen
 Refined model
 Capacity configuration

ABSTRACT

To further explore the multi-energy complementary potential on multi-time scales under variable operating conditions, a refined modeling and collaborative configuration method for Electric-Hydrogen-Thermal-Gas Integrated Energy Systems (EHTG-IES) with hybrid energy storage system (HESS) is proposed in this paper. To commence with, an advanced operation model for the EHTG energy conversion equipment is formulated by incorporating their nonlinear operating characteristics under variable operating conditions. Next, the distinct features of HESS with different energy medium are accurately depicted with various effective linear-reduction and relaxation strategies. Then, the coupling design day method and the intra-day and inter-day state superposition strategy are combined to efficiently model the time horizon. Lastly, a co-optimal configuration model of the EHTG-IES is devised, with the aim of minimizing total annual cost. The case study validates that the refined modeling of coupled components leads to a 3.18% reduction in cost and 5.05% reduction in carbon emissions significantly. This paper also assessments the synergy and substitution benefits of multiple low-carbon technologies and finds that diurnal and seasonal hydrogen storage have a large part of overlapping roles, and hydrogen-based system contributes a deeper utilization of seasonal thermal storage. The sensitivity analysis

* Corresponding author at: School of Economics and Management, North China Electric Power University, Beijing 102206, China.

E-mail address: 120212206029@ncepu.edu.cn (H. Dong).

indicates that the current carbon tax policy has a negligible impact on the carbon emissions, equivalent to about 1% of the gas price, but appropriately increasing attention on low carbon allows for an emission decrease of 28.62% at a cost increase of 4.38%.

Nomenclature		<i>Variables</i>
<i>Abbreviations</i>		
EHTG	Electric-Hydrogen-Thermal-Gas	<i>N</i> Number
IES	Integrated Energy System	<i>I</i> Current
HESS	Hybrid Energy Storage System	<i>U</i> Voltage
PV	Photovoltaic	<i>T</i> Temperature
WT	Wind Turbine	<i>v</i> Wind speed
CHP	Combined Heat and Power	<i>H</i> Thermal Power
AWE	Alkaline Water Electrolyzer	<i>P</i> Electric Power
PEM	Proton Exchange Membrane	<i>V</i> Gas flow rate
FC	Fuel Cell	<i>u</i> Signal for the start/stop status
ME	Methanation Equipment	<i>y/z</i> Operating variables for start/stop
DES	Diurnal Energy Storage	<i>p</i> Pressure
SES	Seasonal Energy Storage	<i>i</i> Current density
STS	Seasonal Thermal Storage	<i>S</i> Stored energy
SHS	Seasonal Hydrogen Storage	<i>E</i> Heat losses of thermal storage
MILP	Mixed Integer Linear Programming	<i>W</i> Installed capacity
SOC	State of Charge	<i>θ</i> Equivalent variable for representing Number * Real-time temperature
EHC	Electric-Hydrogen Coupling	
DEES	Diurnal Electric Energy Storage	
DTS	Diurnal Thermal Storage	
DHS	Diurnal Hydrogen Storage	
EES	Electric Energy Storage	
TS	Thermal Storage	
HS	Hydrogen Storage	
<i>Indices</i>		
sc/pm	Short-Circuit/Peak state	$\zeta, \varsigma, \xi, \Upsilon$
ae	Ambient	<i>A</i>
rated	Rated	Ψ
real	Real-time	λ
in/out	Cut-in/ Cut-out	<i>M</i>
on/off	Strat-up/Shutdown	M^q
up/down	Load-increase/ Load-reduction	M^v
coal/gas	Coal/gas	<i>R</i>
cell	Cell	μ_F
rev/nernst	Reversible/Nernst	γ
act/Ω/con	Activation/Ohmic/Differential	η
$H_2/O_2/Air$	Hydrogen/Oxygen/Air	τ
total/gen	Total energy consumption/generation	κ
pre	Material preheating losses	<i>v</i>
loss	Radiation heat losses	<i>h</i>
low/high	Low/High current	<i>d</i>
min/max	Minimum/maximum	∂
0/T	The initial/final moment	χ
ic/omc	Acquisition/Operating	<i>O</i>
fc/sc/cec	Fuel/strat & stop/carbon tax	<i>L</i>
<i>Cost functions</i>		
k_{ic}	Unit acquisition cost	k_{gas}
k_{fix}	Annual fixed cost coefficient	k_c
k_{var}	Unit variable O&M cost	<i>SC</i>
ρ	Inflation rate	
<i>Parameters</i>		
<i>f</i> Correction factor of PV		
<i>r</i> Light intensity		
<i>c</i> Fitting factor for CHP		
<i>G</i> Gas constant		
<i>F</i> Faraday constant		
<i>v</i> Number of electrons transferred		
ΔG Change in Gibbs energy		
ΔS Reaction enthalpies		
$\zeta, \varsigma, \xi, \Upsilon$ Empirical parameter for FC and AWE		
<i>A</i> Effective surface area		
Ψ Water content		
λ Thickness		
<i>M</i> Lower calorific value		
M^q Molar mass		
M^v Molar volume		
<i>R</i> Thermal resistance		
μ_F Faradaic efficiency		
γ Self-discharge rate		
η Efficiency of charging/discharging		
τ Power-capacity coefficient		
κ Breakpoint of EES		
<i>v</i> Volume		
<i>h</i> Convective heat transfer coefficient		
<i>d</i> Density		
∂ Specific heat capacity		
χ Thermal insulation index		
<i>O</i> Normalized output coefficient		
<i>L</i> Lifetime		
k_{gas} Gas price		
k_c Carbon tax		
<i>SC</i> Unit start-up/stop cost		

1. Introduction

The double pressure of the environment and climate is prompting the transition to a cleaner and lower carbon global power system, and China is in a critical period of building a power network based on renewable energy. The core problem faced by Chinese energy transformation is how to steadily increase the penetration rate of clean energy and untap the potential of multi-energy interaction on multi-time scales on the premise of ensuring the safe and stable energy supply. Electricity-Hydrogen-Thermal-Gas Integrated Energy System (EHTG-IES) with Hybrid Energy Storage System (HESS) integrates multi-type novel low-carbon technologies and multi-energy conversion and storage devices, realizes the spatio-temporal complementary and coupling of different forms of energy, and is a prominent solution [1,2]. A detailed system model is essential to make optimal decisions on the operation and planning of EHTG-IESs with multiple low-carbon technology coupling [3]. In this paper, the refined modeling and co-optimal configuration of EHTG-IES are discussed with an emphasis, which integrates multi-energy and multi-time scale HESS to realize efficient decarbonization and the coordinated dispatch of dynamically interconnected and flexibly cycled electricity, hydrogen, thermal and gas networks.

The key feature of EHTG-IES lies in the multidirectional transfer of energy flows and the decoupling of multi-energy production and supply, which actually occurs in the system's energy conversion and storage equipment. Further analysis of the technical and economic performance of different devices in EHTG-IES and the translation of their operational characteristics into mathematical models are the basis for exploring the mechanism of multi-energy coupling in EHTG-IES and realizing efficient low-carbon dispatch [4,5]. A large number of scholars [4–7] have conducted research on the application of various energy conversion equipment in IES, such as Photovoltaic (PV) panels, Wind Turbines (WT), Combined Heat and Power (CHP) unit, Alkaline Water Electrolyzer (AWE), Proton Exchange Membrane Fuel Cell (PEMFC), and Methanation Equipment (ME), etc. However, all of these studies preliminarily characterized the conversion of different energy sources (such as solar energy, wind, electricity, thermal, natural gas, hydrogen, etc.) with the assumption that the energy efficiency of equipment was a constant, which in fact varied with load rate and temperature [8]. Therefore, the above research have not been able to describe the complex dynamic characteristics inside the equipment accurately, and it is difficult to guarantee the reliability of their energy flow solutions.

To characterize the detailed features of coupled elements, clarify the dynamic operation process, and improve the control capability of IES, related studies are gradually extending from the steady-state study to dynamic processes. Milan [3] modeled the nonlinear part-load efficiency curve for CHP and proposed a linearized expression to improve the optimization efficiency. On this basis, Zhou [9] further introduced the off-design characteristics and part-load efficiency curves of gas engines, gas boilers, and absorption chillers. The results showed that the detailed characteristics of coupled components caused about a 4% deviation from the optimal cost. Given the problem that only backpressure conditions are modeled for CHP in above studies, while variable conditions such as start-stop and extraction steam regulation are ignored, Li [10] conducted detailed modeling of the thermoelectric feasible domain and fuel consumption of CHP, which significantly improved the flexibility of IES. The results showed that CHP would not only operate under back pressure but also in pure condensing condition, depending on the matching of load and unit output. Ebrahimi [11] presented a waste heat utilization strategy for PEMFC based on analyses of electrothermal properties and internal reaction characteristics and verified the efficiency of the strategy. By adjusting the temperature of AWE to change its electrical and/or thermal power, Li [12] established an electric-thermal-hydrogen model for AWE. Pan [1] constructed a refined model that considers the nonlinear characteristics of PEMFC and AWE under variable operating conditions, which enables further utilization of waste heat and significantly improves the economy of IES. Gabrielli [13]

established a detailed thermodynamic model for PEMFC based on a first-principle approach to represent the dynamic features of PEMFC under various operating conditions, and adopted piecewise affine to describe the conversion performance. This brings enlightenment to this study. Some literature [7,14] includes the heat generated in the stage of methanation as one of the output energies, since this step of the chemical reaction is highly exothermic. Burrin [15] conducted a techno-economic evaluation of capturing and utilizing the excess heat emitted by ME and concluded that the levelized cost of energy was reduced.

Scholars have demonstrated the benefits of refined modeling and utilizing multi-type energy conversion equipment for electricity, thermal, hydrogen, and natural gas. However, most of the previous studies were limited to modeling only a single or a few devices for refinement, and the rest of the devices adopted incomplete constraints and simply used a single-segment straight line as the output mapping. The inherent physical properties of these devices are neglected, resulting in a gap between simulation and the real thermodynamic process. With the large number of energy conversion equipment in EHTG-IES, it is important to model the detailed characteristics of these equipment and examine in detail the multi-energy complementary potential under variable operating conditions. In addition, a similar phenomenon is observed for the energy storage devices in IES.

Electric, thermal, and hydrogen energy storage can provide an economical and reliable response to smooth short-term load fluctuations and eliminate seasonal source-load mismatch [16,17], while HESS with a combination of multi-type energy storage has more outstanding techno-economic performance. Evins [18] proposed a unified model for energy storage devices with different forms of energy that considers self-discharge behavior and the continuous change in State of Charge (SOC). Le [16] carried out optimization of the design and operation of HESS with both electric and hydrogen energy media and clarified the advantages of HESS over single energy storage for co-dispatch with renewable energy sources. Jia [19] characterized the behavior of an electric-hydrogen HESS using a unified energy storage model to achieve an optimal configuration of HESS size, which improved CHP operating conditions and enhanced system economics and carbon emission reduction. Petkov [20] investigated the interplay of batteries, thermal storage, and hydrogen storage technologies over various district topologies in central Europe. Bahlawan [21] investigated the synergistic benefits of electric-thermal HESS with PV and claimed that HESS would significantly reduce the CO₂ emissions of the system.

However, the above studies gave limited consideration to the energy medium of HESS, which is an essential difference from the EHTG-IES proposed in this paper. In the EHTG-IES, the variety of electric-thermal-hydrogen energy conversion devices implies a complex multi-energy flow coupling. It emphasizes the importance of thermal energy and hydrogen, which can be energy sources with a status equal to that of electricity. Moreover, the studies mentioned above adopted the unified model to describe HESS and failed to highlight the distinguishing characteristics of energy storage devices with different energy sources.

To date, only a few works have been conducted for refined modeling on different characteristics of HESS due to the complexity of modeling and calculation. Allan [22] verified the dynamic nonlinear relationship between the heat loss efficiency of a thermal storage device and the real-time temperature of the working medium. They stated that simplifying the device efficiency to a constant would cause deviations in the thermal storage regulating strategy. Luo [23] constructed a semi-analytical model of a thermal storage tank considering the dynamic heat loss efficiency based on structural parameters to realize operational control and optimization of renewable-energy-based district heating systems. Steen [24] similarly investigated the dynamic heat loss in thermal storage tanks and proposed a two-temperature simplified model to circumvent the endogenous optimization problem while approximately tracking the real-time heat loss. Mukherjee [25] demonstrated that the power consumption of hydrogen compression in the hydrogen storage tank, the hydrogen charging rate, and the real-time pressure inside the

hydrogen storage tank are multivariate nonlinear. WU [26] highlighted that the existing constant efficiency models need to be sufficiently refined to characterize energy storage efficiency. The authors constructed a dynamic charge/discharge efficiency model for electric storage and proved to verify the benefits of the refined characteristics of energy storage for renewable energy consumption. Ren [27] suggested that the differential dynamic characteristics of HESS due to physical/chemical processes were the key to optimal modeling of EHTG-IES. However, to the best of our knowledge, there are still no optimization studies that integrate the above dynamic and refined characteristics of HESS. The main reason for the above problem is that the above fine features will make the planning model non-convex. Heuristic algorithms and machine learning are the main paths for solving nonconvex problems [28], but they hardly guarantee the optimality of the solution [29]. In contrast, mixed integer linear programming (MILP) allows for the exact optimal solution to be obtained by mature algorithms. Therefore, suitable and effective linear order-reduction and relaxation strategies for the refined characteristics of HESS are urgently needed.

In addition, EHTG-IES with a high penetration of renewable energy requires Diurnal Energy Storage (DES) to provide enough reserve capacity to absorb excess power within a day and Seasonal Energy Storage (SES) to solve the imbalance of seasonal energy supply and demand on a long timescale. Therefore, differential modeling and co-optimization of DES and SES have drawn increasing attention in EHTG-IES optimal dispatching research. Lyden [30] considered Seasonal Thermal Storage (STS) as a supplement and adjustment to the heating system, showing the potential to reconcile the seasonal mismatch between heat supply and demand and further improve the overall efficiency of the heating system. Because Seasonal Hydrogen Storage (SHS) is one of the few technologies capable of storing seasonal energy without experiencing considerable self-discharge, Wang [31] believed that it is a potential technology to contribute to the decarbonization of IES [32].

Nevertheless, Chen [2] highlighted the intractability of seasonal source-load mismatch and argued that the critical issue in tapping the potential of SES is how to deal with intra-seasonal and inter-seasonal optimization. Particularly, co-optimizing the dynamic operation of DES and SESs has proven to be difficult to solve within the required time due to the enormous number of decision variables in the model [32]. With the intent of characterizing the seasonal source-load mismatch, Sánchez [33] proposed a multiscale time representation method, but it used a full-time series to model the system. Moreover, Pu [34] designed a clustering and scene generation method based on eigenvalues to focus on the primary causes and simplify the dispatching models. The authors described the dispatch problem in SES as a MILP model. Based on this model, Gabrielli [35] achieved the co-optimization of short- and long-term thermal storage, with which Chen [36] introduced short-time and seasonal electric storage into the carbon capture system of power plants, resulting in a 2.15% reduction in total cost. Based on this time-granularity grid, Bahlawan [21] explored the synergistic effect of long- and short-term thermal energy storage with renewable energy plants. However, these aggregated typical periods are modeled independently and cannot exchange energy. Weimann [37] believed that the above pathway also ignored extreme events and proposed a multi-timescale method that models different technologies at various temporal scales to develop systems with a high penetration of renewable energy. However, the continuous hourly SOC of HESS in the whole year cannot be obtained, which means the spatio-temporal granularity is limited. Gabrielli [38] proposed a time horizon modeling method named as ‘Coupling Design Days’, using design days to derive the total time horizon, to describe the hourly state in a typical period and the interactive coupling state among interday and intraday. The results show that it not only allows the initial and end levels of the SOC of HESS to be inconsistent within discrete typical days/weeks, but also reveals the seasonal storage effect of both DES and SES. Nevertheless, the method is so computationally intensive that its computation time often exceeds several hours of CPU time. Notably, Kotzur [39] proposed a time series aggregation method that significantly circumvents the variable increase of repetitive states within a typical period by means of a mathematical

description of the storage inventory based on the superposition of inter-period and intra-period states. There is significant value in combining these two strategies, but it seems that no study has done so as far we know.

Power system planning for the ‘dual carbon target’ requires decision analysis for system development in the context of numerous low-carbon technologies coupling [40]. Energy system modeling is a commonly used method to provide policy recommendations and insight into the transformation pathways of energy systems [8]. Table 1 summarizes the low-carbon technologies and their modeling form applied in the above research. It is not difficult to discover that the planning models in the above studies mainly focus on a single or few novel low-carbon technologies and model the corresponding equipment elaborately, while the remaining low-carbon technologies are only roughly modeled or even not regarded. This implies that the potential of the remaining low-carbon technologies has not been profoundly exploited, both from the perspective of the technologies themselves and multi-technology coupling. Although the above studies have made an outstanding contribution to quantifying and clarifying the role played by each low-carbon technology in the low-carbon transition of the power system in the context of the coupling of multiple low-carbon technologies, more comprehensive and detailed models and mathematical analysis are required to facilitate the understanding of how technologies interact, and how synergies can be exploited. In addition, the low open-source availability of the frameworks in practice often leads to low interpretability and transparency of energy modeling system configurations.

In this context, this paper aims to develop refined modeling for various novel low-carbon technologies and propose a co-optimization method for EHTG-IES with HESS. In this study, the co-optimization is implemented with the goal of achieving minimum annual total costs to enhance the integration of energy conversion and storage technologies, the complementary of energy storage technologies with different energy mediums, as well as the dynamic interconnectivity of DES and SES. The research route of this paper is shown in Fig. 1. Besides, the research data and code will be open-sourced at [41]. The critical objectives of this work are as follows:

(1) All low-carbon technologies applied to EHTG-IES are finely modeled. The multi-energy complementary potential on multi-time scales under variable operating conditions of various low-carbon technologies is exploited.

(2) The planning optimization model of EHTG-IES is implemented with sensitivity analysis, taking into account different intensities of decarbonization, explaining the planning strategies implied by the optimization results, and quantitatively investigating the coupling effects among multiple technologies to provide decision support for low-carbon transformation of power systems in the context of the integration of many novel low-carbon technologies.

The original contributions of this research are as follows:

(1) A holistic and refined operation model in variable operating conditions is developed by comprehensively considering the nonlinear operation characteristics of EHTG-IES’s energy conversion equipment, so as to achieve better quality and higher efficiency of EHTG-IES on the basis of reliable planning results.

(2) A refined model of HESS containing multi-energy mediums (electricity, hydrogen, and thermal) is constructed to describe the different and dynamic characteristics in the physical and chemical processes of multi-energy storages and ensure the equal status of electricity, hydrogen, and thermal in EHTG-IES. Besides, this paper develops effective linear order-reduction and relaxation strategies for the refined characteristics of HESS.

(3) A refined model of HESS accounting for multi-time scales is constructed, which utilizes the coupling design days method to solve the problem of limited flexibility of the SOC of HESS on long timescales and realize the co-optimization of DES and SES, and employs the mathematical description for inventories of multi-timescale energy storage based on the superposition of interday and intraday states for improving the optimization efficiency.

Table 1

Literature review of low-carbon technologies and their model applied in an IES.

Ref.	Energy conversion equipment						Energy storage devices				
	PV	WT	CHP	PEMFC	AWE	P2G	DEES	DTS	DHS	STS	SHS
Milan [3]	o	x	/	x	x	x	o	o	x	x	x
Liu [4]	/	/	o	x	x	x	o	x	x	x	x
Zhou [5]	o	o	o	o	o	x	o	x	o	x	x
Guo [6]	/	x	/	x	x	x	/	o	x	x	x
Yang [7]	x	x	/	x	o	/	x	x	x	x	x
Zhou [9]	x	x	/	x	x	x	x	o	x	x	x
Li [10]	x	o	/	x	x	o	o	o	x	x	x
Ebrahimi [11]	x	x	x	/	x	x	x	x	x	x	x
Li [12]	o	o	/	x	/	x	x	x	o	x	o
Gabrielli [13]	x	x	x	/	x	x	o	o	o	x	x
Schiebahn [14]	x	x	x	x	/	/	x	x	x	x	x
Burrin [15]	x	x	x	x	/	x	x	x	x	x	x
Le [16]	o	x	x	/	/	x	/	x	o	x	o
Gabrielli [17]	x	x	x	x	x	x	x	/	x	x	/
Evins [18]	o	x	x	x	x	x	o	o	o	x	x
Jia [19]	/	/	/	x	/	x	o	x	/	x	x
Petkov [20]	o	o	x	/	x	x	o	o	o	o	o
Bahlawan [21]	/	x	x	x	x	x	o	o	x	/	x
Allan [22]	x	x	x	x	x	x	/	x	/	x	x
Luo [23]	x	x	x	x	x	x	/	x	/	x	x
Steen [24]	o	x	o	x	x	x	o	/	x	x	x
Mukherjee [25]	x	x	x	o	o	/	x	x	o	x	o
WU [26]	x	/	x	x	x	x	/	x	x	x	x
Lyden [30]	o	o	o	o	o	x	o	/	o	/	o
Wang [31]	o	o	o	/	/	x	o	o	/	x	/
Petkov [32]	o	o	x	/	x	x	o	o	o	o	o
Sánchez [33]	/	/	o	x	/	/	x	x	x	x	x
Pu [34]	o	x	o	/	/	x	x	o	/	x	/
Gabrielli [35]	x	x	o	x	x	x	x	x	/	x	/
Chen [36]	o	o	/	/	/	/	/	o	x	x	x
Weimann [37]	o	x	o	/	x	x	x	x	o	x	o
Gabrielli [38]	o	x	x	/	/	x	x	o	o	o	o
Kotzur [39]	/	/	/	o	o	x	o	o	o	o	o
This paper	/	/	/	/	/	/	/	/	/	/	/

Note: x means that the device is not considered in that study, o means that it is modeled simplistically, and / means that it is modeled in detailed.

(4) A co-optimization method of EHTG-IES with the refined model is proposed to investigate the synergistic and complementary benefits of various low-carbon technologies and the technical economics of each energy subsystem under different low-carbon target attention. In addition, the effect of source-load endowment on the planning of EHTG-IES with HESS is examined by adjusting the source-load temporal sequence and duration.

2. Refined mathematical model in variable operating conditions of multi-type energy conversion equipment

The detailed topology and the basic procedures strategy of EHTG-IES are summarized in Fig. 2. The performance and operating range of EHTG-IES depend on the characteristics and coordinated linkage of the energy conversion equipment in the system. A refined description for the technical and economic performance of the different devices in EHTG-IES will help the optimization model for a lean allocation of resources. Therefore, the next part of the paper will be devoted to refined mathematical modeling of different devices.

2.1. Primary energy conversion subsystem

2.1.1. Renewable energy generation subsystem

The actual power generated by PV panels is mainly influenced by the intensity of solar radiation and ambient temperature, as shown in Fig. 3 and as calculated by the following equations [6,42]:

$$P^{\text{PV}} = N^{\text{PV}} I^{\text{PV}} U^{\text{PV}} f_{\text{T}}^{\text{PV}} f_{\text{D}}^{\text{PV}} \quad (1)$$

$$I^{\text{PV}} = I_{\text{sc}}^{\text{PV}} \left(r_{\text{ae}} / r_{\text{rated}}^{\text{PV}} - 1 \right) + I_{\text{pm}}^{\text{PV}} \quad (2)$$

$$U^{\text{PV}} = U_{\text{pm}}^{\text{PV}} \left(1 + 0.0593 \lg \left(r_{\text{ae}} / r_{\text{rated}}^{\text{PV}} \right) \right) \quad (3)$$

$$f_{\text{T}}^{\text{PV}} = 1 - (T_{\text{real}}^{\text{PV}} - T_{\text{rated}}^{\text{PV}}) / 200 \quad (4)$$

$$T_{\text{real}}^{\text{PV}} = T_{\text{ae}} + 30r_{\text{ae}} / 800 \quad (5)$$

where N^{PV} is the number of panels; I^{PV} , $I_{\text{sc}}^{\text{PV}}$, $I_{\text{pm}}^{\text{PV}}$ represent real-time current, short-circuit current, and peak current respectively; U^{PV} , $U_{\text{pm}}^{\text{PV}}$ refer to real-time voltage and peak voltage; f_{T}^{PV} , f_{D}^{PV} are the temperature and dust correction factor; r_{ae} , $r_{\text{rated}}^{\text{PV}}$ refer to the real-time light intensity and rated light intensity; T_{ae} is the ambient temperature, $T_{\text{real}}^{\text{PV}}$, $T_{\text{rated}}^{\text{PV}}$ are the actual temperature and rated temperature of the PV panel.

The pitch angle of WT is adopted in this work, and the actual power of the wind turbine is mainly determined by the cut-in and cut-out wind speed, as shown in Fig. 3. In phases a and b, the pitch angle is constant at 0 to obtain the maximum wind energy utilization factor. In phase a, the wind has insufficient kinetic energy to drive the rotation of blades, while the blade speed increases with the wind speed in phase b. The power output shows a cubic relation with the wind speed. The pitch angle increases in phase c to reduce the wind energy utilization factor to ensure a constant blade speed. In stage d, the wind speed is more than the cut-off speed, and the pitch angle adjustment is not enough to ensure the safe operation of WT. WT is hence stops resulting no output power [19]. The detailed model is as follows [4]:

$$P^{\text{WT}} = \begin{cases} 0 & \text{if } v(t) \leq v_{\text{in}} \text{ or } v(t) \geq v_{\text{out}} \\ P_{\text{rated}}^{\text{WT}} (v^3 - v_{\text{in}}^3) / (v_{\text{rated}}^3 - v_{\text{in}}^3) & \text{if } v_{\text{in}} \leq v(t) \leq v_{\text{rated}} \\ P_{\text{rated}}^{\text{WT}} & \text{if } v_{\text{rated}} \leq v(t) \leq v_{\text{out}} \end{cases} \quad (6)$$

where P^{WT} and $P_{\text{rated}}^{\text{WT}}$ refer to the real-time power and rated power of a

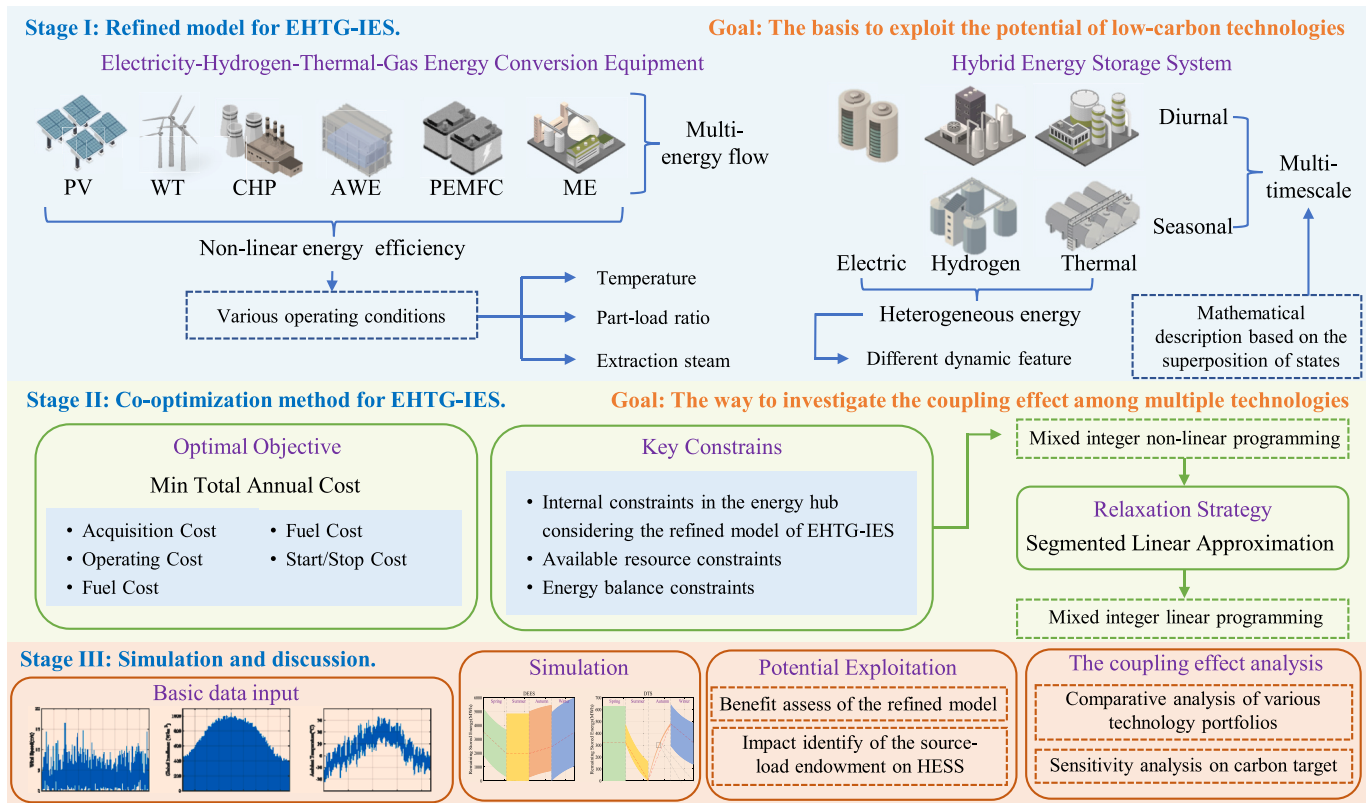


Fig. 1. Research route of this study.

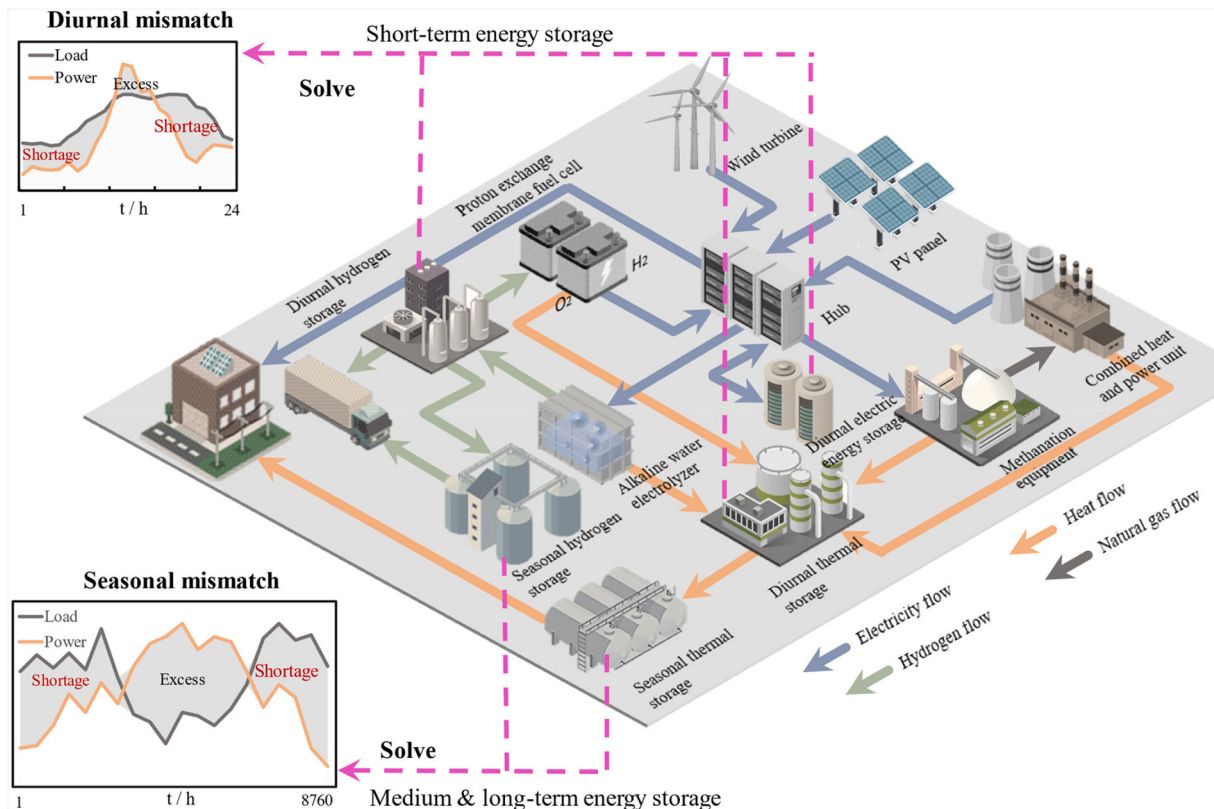


Fig. 2. Detailed topology and basic procedures strategy of EHTG-IES.

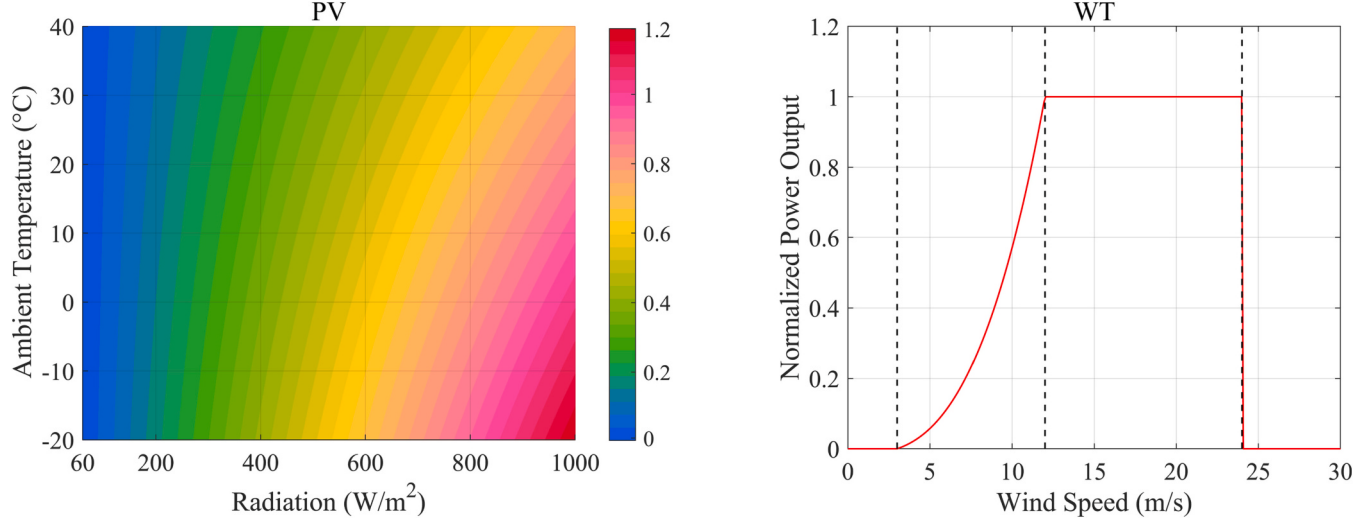


Fig. 3. Renewable energy subsystem technology output performance under different resource conditions.

single WT; v , v_{in} , v_{out} and v_{rated} represent the actual wind speed, cut-in wind speed, cut-out wind speed, and rated wind speed, respectively.

2.1.2. Combined heat and power subsystem

Previous studies [5,12,16] have mostly used back-pressure CHP units, whose thermoelectric coupling would reduce system flexibility, so this paper adopts an extraction condensing unit. To improve the accuracy of the flexible description of CHP, the feasible operation region is characterized in this paper, as shown in Fig. 4. A convex polygon can represent the feasible operation region. The technical thermoelectric output constraint is shown in Eqs. (7-8), the ramp rate limit is characterized as the supply creep constraint when converting the thermoelectric output to pure condensing conditions, as shown in Eqs. (9-10), Eq. (11) defines the relationship between start-stop operation and start-stop state, and Eqs. (12-13) further specifies the start-stop constraint. Eq. (14) is the natural gas consumption in quadratic function [36,43].

$$0 \leq H_t^{CHP} \leq H_{\max}^{CHP} u_t^{CHP} \quad (7)$$

$$\max\{P_{\min}^{CHP} u_t^{CHP} - c_{v2} H_t^{CHP}, K u_t^{CHP} + c_m H_t^{CHP}\} \leq P_t^{CHP} \leq P_{\max}^{CHP} u_t^{CHP} - c_{v1} H_t^{CHP} \quad (8)$$

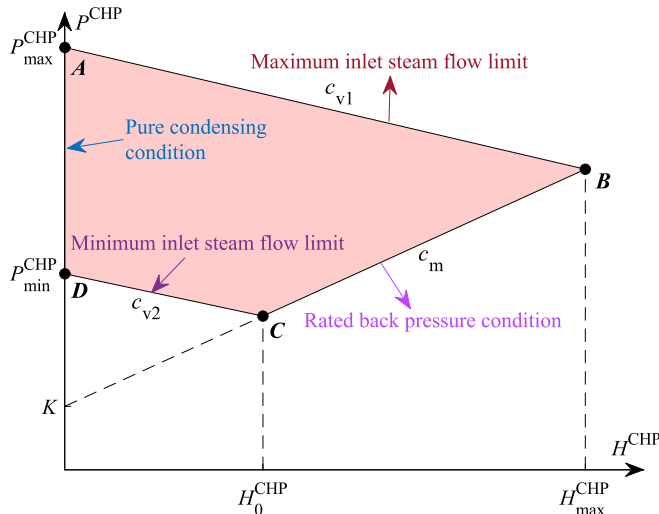


Fig. 4. Feasible operating region of the extraction condensing CHP.

$$\hat{P}_t^{CHP} = P_t^{CHP} + c_m H_t^{CHP} \quad (9)$$

$$-P_{\text{off}}^{CHP} z_t^{CHP} - P_{\text{down}}^{CHP} u_t^{CHP} \leq \hat{P}_t^{CHP} - \hat{P}_t^{CHP} \leq P_{\text{up}}^{CHP} u_t^{CHP} + P_{\text{on}}^{CHP} y_t^{CHP} \quad (10)$$

$$u_t^{CHP} - u_{t-1}^{CHP} = y_t^{CHP} - z_t^{CHP} \quad (11)$$

$$\sum_{t=\max(p-T_{\text{on}}^{CHP}+1,1)}^T y_t^{CHP} \leq u_T^{CHP} \quad (12)$$

$$\sum_{t=\max(p-T_{\text{on}}^{CHP}+1,1)}^T z_t^{CHP} \leq 1 - u_T^{CHP} \quad (13)$$

$$V_{\text{gas}}^{CHP} = \frac{M_{\text{coal}}}{M_{\text{gas}}} \left[c_0 + c_1 P^{CHP} + c_2 H^{CHP} + c_3 (P^{CHP})^2 + c_4 P^{CHP} H^{CHP} + c_5 (H^{CHP})^2 \right] \quad (14)$$

where V_{gas}^{CHP} is the natural gas consumption rate of CHP at time t ; H_t^{CHP} , P_t^{CHP} are the heat and power production of CHP; \hat{P}_t^{CHP} is the equivalent electrical output; H_{\max}^{CHP} is the backpressure heating limit; P_{\max}^{CHP} , P_{\min}^{CHP} refer to the upper and lower limits of power in pure condensing conditions; c_{v1} , c_{v2} , c_m refer to the elasticity coefficients of heat production to power generation under maximum steam inlet, minimum steam inlet and back pressure conditions; c_j is the coal consumption fitting factor; P_{up}^{CHP} , P_{down}^{CHP} , P_{on}^{CHP} , P_{off}^{CHP} refer to the upper limits of load increase, load reduction, start-up and shutdown rates; u_t^{CHP} is the Boolean variables for the start/stop status; y_t^{CHP} , z_t^{CHP} are the Boolean variables for start-up and shutdown operation; T_{on}^{CHP} , T_{off}^{CHP} are the minimum start-up and shutdown duration; M_{coal} , M_{gas} indicate the minimum heat of combustion value for standard coal and natural gas.

2.2. Secondary energy conversion subsystem

2.2.1. Electric-hydrogen coupling subsystem

This paper selects PEMFC and AWE as Electric-Hydrogen Coupling (EHC) subsystem for reasons of technology maturity and cost. Their sophisticated operating features are specified as a unique nonlinear polarization curve, as shown in Fig. 5. The energy conversion efficiency of this subsystem is affected by the input power and the work temperature. The efficiency is only 60%–70% at present, while the rest of the energy is dissipated chiefly in the form of heat, and the waste heat has a large considerable value. As a result, it is necessary to establish an electric-hydrogen-thermal refinement model for EHC.

Regarding electricity, PEMFC incurs polarization losses during

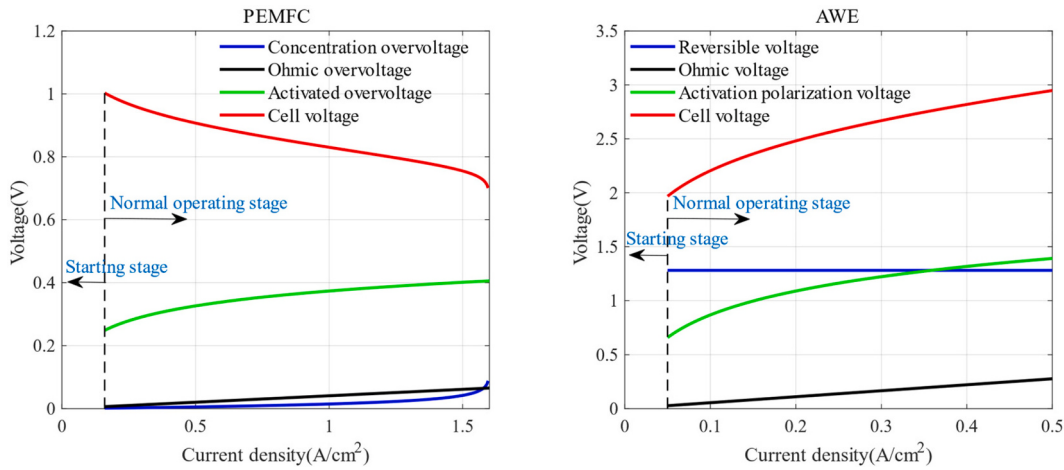


Fig. 5. The nonlinear polarization curves of PEMFC and AWE.

operation, mainly in terms of activation, concentration, and ohmic polarization [11,44–46]. The voltage of FC is calculated in Eq. (15).

$$\left\{ \begin{array}{l} U_{\text{cell}}^{\text{FC}} = N^{\text{FC}} U_{\text{cell}}^{\text{FC}} \\ U_{\text{cell}}^{\text{FC}} = U_{\text{nernst}} - U_{\text{act}}^{\text{FC}} - U_{\text{ohm}}^{\text{FC}} - U_{\text{con}}^{\text{FC}} \\ U_{\text{nernst}} = \{ \Delta G + \Delta S(T^{\text{FC}} - T_{\text{ae}}) + GT^{\text{FC}} [\ln(p_{\text{H}_2}) + 0.5\ln(p_{\text{O}_2})] \} / (vF) \\ U_{\text{act}}^{\text{FC}} = \xi_1 + \xi_2 T^{\text{FC}} + \xi_4 T^{\text{FC}} \ln(i^{\text{FC}} A^{\text{FC}}) + \xi_3 T^{\text{FC}} \ln(p_{\text{O}_2}) / [5.08 \times 10^6 \exp(-498/T^{\text{FC}})] \\ U_{\text{ohm}}^{\text{FC}} = i^{\text{FC}} \Psi^{\text{FC}} / [(0.005139 \lambda^{\text{FC}} - 0.00326) \exp(1268(1/303 - 1/T^{\text{FC}}))] \\ U_{\text{con}}^{\text{FC}} = [\ln(A^{\text{FC}} i_{\text{rated}}^{\text{FC}}) - GT^{\text{FC}} \ln(1 - i^{\text{FC}} A^{\text{FC}})] / (vF) \end{array} \right. \quad (15)$$

where, U^{FC} refers to the voltage of FC; N^{FC} are the number of series connections in the FC stack; $U_{\text{cell}}^{\text{FC}}$ is the cell voltage; U_{nernst} is the thermodynamic electric potential; $U_{\text{act}}^{\text{FC}}$, $U_{\text{ohm}}^{\text{FC}}$, and $U_{\text{con}}^{\text{FC}}$ are the activation, ohmic, differential polarization loss; ΔG is the change in Gibbs energy; ΔS is the change in entropy; T^{FC} is the temperature of FC; G is the gas constant; p_{H_2} refers to the partial pressure of hydrogen at the anode catalyst interface; p_{O_2} is the partial pressure of oxygen at the cathode catalyst interface; v refers to the number of electrons transferred per reaction; F is the faraday constant; ξ_n is the empirical parameter of the activation over-voltage, $n = 1, 2, 3, 4$; i^{FC} is the current density of FC; $i_{\text{rated}}^{\text{FC}}$ is the rated current density of FC; A^{FC} , Ψ^{FC} , λ^{FC} are the effective area, water content, and thickness of PEM.

The hydrogen consumption rate of FC is calculated in Eq. (16).

$$V_{\text{H}_2}^{\text{FC}} = i^{\text{FC}} N^{\text{FC}} M_{\text{H}_2}^q A^{\text{FC}} / (vF) \quad (16)$$

where, $M_{\text{H}_2}^q$ is the molar mass of hydrogen.

The power generation of FC is shown in Eq. (17).

$$P^{\text{FC}} = U^{\text{FC}} i^{\text{FC}} A^{\text{FC}} \quad (17)$$

In terms of thermal, PEMFC has material preheating losses and radiation heat losses. The thermal balance equation of FC is shown in Eq. (18).

$$\left\{ \begin{array}{l} H^{\text{FC}} = P_{\text{total}}^{\text{FC}} - P^{\text{FC}} - H_{\text{pre}}^{\text{FC}} - H_{\text{loss}}^{\text{FC}} \\ P_{\text{total}}^{\text{FC}} = V_{\text{H}_2}^{\text{FC}} M_{\text{H}_2} M_{\text{H}_2}^v / M_{\text{H}_2}^q \\ H_{\text{pre}}^{\text{FC}} = \left(V_{\text{H}_2}^{\text{FC}} c_{\text{H}_2} + V_{\text{Air}}^{\text{FC}} c_{\text{Air}} \right) (T_{\text{material}}^{\text{FC}} - T_{\text{ae}}) \\ V_{\text{Air}}^{\text{FC}} = V_{\text{H}_2}^{\text{FC}} / \lambda_{\text{Air}}^{\text{H}_2} \\ H_{\text{loss}}^{\text{FC}} = (T^{\text{FC}} - T_{\text{ae}}) / R^{\text{FC}} \end{array} \right. \quad (18)$$

where, H^{FC} is the external heating power of FC. $P_{\text{total}}^{\text{FC}}$ is the total energy consumption of FC; $H_{\text{pre}}^{\text{FC}}$, $H_{\text{loss}}^{\text{FC}}$ are the preheating heat consumption and the radiation heat loss; M_{H_2} , $M_{\text{H}_2}^v$ are the lower calorific value and molar volume of hydrogen; c_{H_2} , c_{Air} are the specific heat capacity of hydrogen and air; $T_{\text{material}}^{\text{FC}}$ refers to the temperature of the used material; $V_{\text{Air}}^{\text{FC}}$ refers to the air consumption rate; $\lambda_{\text{Air}}^{\text{H}_2}$ is the stoichiometry ratio of hydrogen to air; R^{FC} refers to the total thermal resistance of FC.

Considering thermodynamic and resistive effects, the cell voltage of AWE is defined as the sum of the reversible voltage and overpotentials [47] (Eq. (19)).

$$\left\{ \begin{array}{l} U^{\text{AWE}} = N^{\text{AWE}} U_{\text{cell}}^{\text{AWE}} \\ U_{\text{cell}}^{\text{AWE}} = U_{\text{rev}}^{\text{AWE}} + U_{\text{act}}^{\text{AWE}} + U_{\text{ohm}}^{\text{AWE}} \\ U_{\text{rev}}^{\text{AWE}} = U_{\text{rev}0} + GT^{\text{AWE}} (\ln(p^{\text{AWE}}) - \ln(p_{\text{ae}})) / (vF) \\ U_{\text{act}}^{\text{AWE}} = 0.33824 \ln(i^{\text{AWE}} \left[\zeta_1 + \zeta_2 / (T^{\text{AWE}} - 273.15) \right. \\ \left. + \zeta_3 / (T^{\text{AWE}} - 273.15)^2 \right] + 1) \\ U_{\text{ohm}}^{\text{AWE}} = i^{\text{AWE}} (\zeta_1 + \gamma_1 + \zeta_2 (T^{\text{AWE}} - 273.15) + \gamma_2 p^{\text{AWE}}) \end{array} \right. \quad (19)$$

where, U^{AWE} is the voltage of AWE; N^{AWE} the number of series connections in the AWE stack; $U_{\text{cell}}^{\text{AWE}}$ is the cell voltage; $U_{\text{rev}}^{\text{AWE}}$ is the reversible voltage; $U_{\text{act}}^{\text{AWE}}$, $U_{\text{ohm}}^{\text{AWE}}$ are the activation and ohmic polarization overvoltage; $U_{\text{rev}0}$ is the reversible voltage at a temperature of 50 °C and a pressure of 1 atm; T^{AWE} , p^{AWE} are the temperature and pressure of AWE; p_{ae} is the ambient pressure; i^{AWE} is the current density in EL; ζ_n refer to the empirical parameter of activation polarization voltage, $n = 1, 2, 3$; and ζ_n , γ_n are the empirical parameter of ohmic voltage with temperature and with pressure, $n = 1, 2$.

The power consumption of AWE is shown in Eq. (20).

$$P^{\text{AWE}} = U^{\text{AWE}} A^{\text{AWE}} i^{\text{AWE}} \quad (20)$$

where, A^{AWE} is the effective surface area of a single AWE module.

The hydrogen produce rate of AWE is shown in Eq. (21).

$$\left\{ \begin{array}{l} V_{\text{H}_2}^{\text{AWE}} = N^{\text{AWE}} \mu_F i^{\text{AWE}} A^{\text{AWE}} / (vF M_{\text{H}_2}^q) \\ \mu_F = (i^{\text{AWE}})^2 [1.03960 - 0.00104(T^{\text{AWE}} - 273.15)] / [47.864574 \\ - 0.295315(T^{\text{AWE}} - 273.15)] \end{array} \right. \quad (21)$$

where, μ_F is the faradaic efficiency.

Radiative heat loss is the most dominant kind of heat loss [47–49]. The thermal balance equation of AWE is:

$$\left\{ \begin{array}{l} H^{\text{AWE}} = H_{\text{gen}}^{\text{AWE}} - H_{\text{loss}}^{\text{AWE}} \\ H_{\text{gen}}^{\text{AWE}} = P^{\text{AWE}} - V_{\text{H}_2}^{\text{AWE}} M_{\text{H}_2} M_{\text{H}_2}^{\text{v}} / M_{\text{H}_2}^{\text{a}} \\ H_{\text{loss}}^{\text{AWE}} = (T^{\text{AWE}} - T_{\text{ac}}) / R^{\text{AWE}} \end{array} \right. \quad (22)$$

where, H^{AWE} is the heating power of AWE; $H_{\text{gen}}^{\text{AWE}}$, $H_{\text{loss}}^{\text{AWE}}$ are the total heat production of AWE and the radiant heat loss; R^{AWE} refers to the total thermal resistance of AWE.

In addition, PEMFC and AWE are also subject to the following security constraints [49,50]:

$$10\% i_{\text{rated}}^{\text{FC}} \leq i^{\text{FC}} \leq i_{\text{rated}}^{\text{FC}} \quad (23)$$

$$10\% i_{\text{rated}}^{\text{AWE}} \leq i^{\text{AWE}} \leq i_{\text{rated}}^{\text{AWE}} \quad (24)$$

where, $i_{\text{rated}}^{\text{AWE}}$ are the rated current density of AWE.

2.2.2. Power to gas subsystem

ME provides more flexibility in the planning of EHTG-IES by synergistically utilizing residual electricity and hydrogen to produce natural gas. The power used, hydrogen consumption rate, and heat supply power of ME in the methanation reaction stage are defined in Eqs. (38–40) [7], and operational constraints such as ramp-up and output power are characterized in Eqs. (25–29) [51].

$$P^{\text{ME}} = V_{\text{gas}}^{\text{ME}} M_{\text{gas}} / (3600 \eta^{\text{ME}}) \quad (25)$$

$$V_{\text{H}_2}^{\text{ME}} = 4 V_{\text{gas}}^{\text{ME}} \quad (26)$$

$$H^{\text{ME}} = 1000 \lambda^{\text{ME}} V_{\text{gas}}^{\text{ME}} / M_{\text{gas}}^{\text{v}} \quad (27)$$

$$0 \leq P^{\text{ME}} \leq W^{\text{ME}} \quad (28)$$

$$-P_{\text{down}}^{\text{ME}} \leq P_t^{\text{ME}} - P_{t-1}^{\text{ME}} \leq P_{\text{up}}^{\text{ME}} \quad (29)$$

where $V_{\text{gas}}^{\text{ME}}$, $V_{\text{H}_2}^{\text{ME}}$, P^{ME} and H^{ME} are the natural gas generation rate, hydrogen depletion rate, power consumed and heat production power; W^{ME} , η^{ME} are the ME capacity and efficiency; $M_{\text{gas}}^{\text{v}}$ is the molar volume of natural gas; λ^{ME} is the exothermic coefficient of the methanation reaction; $P_{\text{up}}^{\text{ME}}$ and $P_{\text{down}}^{\text{ME}}$ are the ME load and load increase and decrease rate limits.

3. Refined mathematical model for HESS with multi-energy and multi-timescale properties

The HESS constructed in this paper are categorized into DES and SES according to the time scale. Lithium batteries are only used for Diurnal Electric Energy Storage (DEES); heat storage tanks and hydrogen storage tanks are used for both DES and SES. DES focuses on intra-day power interactions, while SES focuses on energy time-shifting across seasons. Therefore, high-pressure hydrogen storage tanks are used for Diurnal Hydrogen Storage (DHS) for frequent interaction with hydrogen-fueled vehicles, medium-pressure tanks are used for SHS; and high-capacity thermal storage tanks are used for STS for efficient and economical inter-seasonal heat migration, low-capacity thermal tanks are used for Diurnal Thermal Storage (DTS).

Energy storage devices with different forms of energy have different physical and chemical dynamic properties during actual operation. In addition, different time scales lead to differences in charging/discharging behavior. Therefore, constructing the HESS with different dynamic characteristics and multi-timescale properties and making them operate in synergy is the focus of this chapter.

3.1. Refined model of HESS with dynamic multi-energy characteristics

3.1.1. Refined model of electric energy storage considering dynamic charge/discharge efficiency

In this paper, electric energy storage consists of a container-type energy storage system with a lithium iron phosphate battery. The performance of Li-battery during charging and discharging is highly related to SOC, the current and voltage. A constant-voltage charging strategy is used in this paper to get close to the optimal charging curve. Then, the dynamic performance of Li-battery performance under this strategy with respect to current and voltage is shown in Fig. 6a [52]. Since the efficiency of Li-battery charging and discharging is mainly affected by the current, this paper only adopts the current intensity as its independent variable. Multiple constant values are used to characterize the dynamic charge/discharge efficiency in order to preserve as much as possible the dynamic operating characteristics of the electric energy storage while ensuring the linearity of the model (shown in Fig. 6b). These typical values are determined by K-means algorithm. Finally, the behavior of the electric energy storage is described by the following linear dynamics:

$$S_t^{\text{EES}} = (1 - \gamma^{\text{EES}}) S_{t-1}^{\text{EES}} + (P_{t-1}^{\text{EES,c,low}} \eta^{\text{EES,c,low}} - P_{t-1}^{\text{EES,d,low}} / \eta^{\text{EES,d,low}}) + (P_{t-1}^{\text{EES,c,high}} \eta^{\text{EES,c,high}} - P_{t-1}^{\text{EES,d,high}} / \eta^{\text{EES,d,high}}) \quad (30)$$

$$S_{\min}^{\text{EES}} \leq S_t^{\text{EES}} \leq S_{\max}^{\text{EES}} \quad (31)$$

$$S_0^{\text{EES}} = S_T^{\text{EES}} \quad (32)$$

$$0 \leq P_{t-1}^{\text{EES,c,low}} \leq \kappa^{\text{EES}} \tau^{\text{EES}} W_{\text{low}}^{\text{EES}} \quad (33)$$

$$0 \leq P_{t-1}^{\text{EES,d,low}} \leq \kappa^{\text{EES}} \tau^{\text{EES}} W_{\text{low}}^{\text{EES}} \quad (34)$$

$$\kappa^{\text{EES}} \tau^{\text{EES}} W_{\text{c,high}}^{\text{EES}} \leq P_{t-1}^{\text{EES,c,high}} \leq \tau^{\text{EES}} W_{\text{c,high}}^{\text{EES}} \quad (35)$$

$$\kappa^{\text{EES}} \tau^{\text{EES}} W_{\text{d,high}}^{\text{EES}} \leq P_{t-1}^{\text{EES,d,high}} \leq \tau^{\text{EES}} W_{\text{d,high}}^{\text{EES}} \quad (36)$$

$$W^{\text{EES}} = W_{\text{low}}^{\text{EES}} + W_{\text{c,high}}^{\text{EES}} + W_{\text{d,high}}^{\text{EES}} \quad (37)$$

where, EES represents electric energy storage; S_t^{EES} is the storage inventories of the EES device at time t ; S_0^{EES} and S_T^{EES} are the stored energy at the initial and final moments of the optimization cycle; S_{\min}^{EES} and S_{\max}^{EES} are the minimum and maximum of the stored energy for EES; $P_t^{\text{EES,c,high}}$ and $P_t^{\text{EES,d,high}}$ are the charge/discharge power under high current intensity; $\eta^{\text{EES,c,high}}$ and $\eta^{\text{EES,d,high}}$ are the responding charging/discharging efficiency; $P_t^{\text{EES,c,low}}$ and $P_t^{\text{EES,d,low}}$ are the charge/discharge power under high current intensity; $\eta^{\text{EES,c,low}}$ and $\eta^{\text{EES,d,low}}$ are the responding charging/discharging efficiency; γ^{EES} is the self-discharge rate; W^{EES} is the installed capacity of EES; $W_{\text{low}}^{\text{EES}}$ is the capacity of EES working under low current intensity state; it is noting that there are two capacity $W_{\text{c,high}}^{\text{EES}}$ and $W_{\text{d,high}}^{\text{EES}}$ for EES working under high current intensity state, because EES will charge and discharge at the same time if there is only one capacity variable for high current intensity state; κ^{EES} refers to the breakpoint for current intensity; τ^{EES} is the power-to-capacity ratio of device.

3.1.2. Refined model of thermal storage considering dynamic self-discharge rates

The thermal energy storage system consists of thermal storage tanks. The energy loss is reflected in two parts:

(i) Heat transfer loss inside the tank: Due to thermal inertia, heat loss arises from mixing hot and cold water in the sloped temperature layer and from the heat transfer between the water and the tank walls. This paper represents this part of the heat loss in terms of heat release/storage efficiency, ignoring the influence of dynamic characteristics such as the flow of liquid inside the accumulator, which is set as a fixed

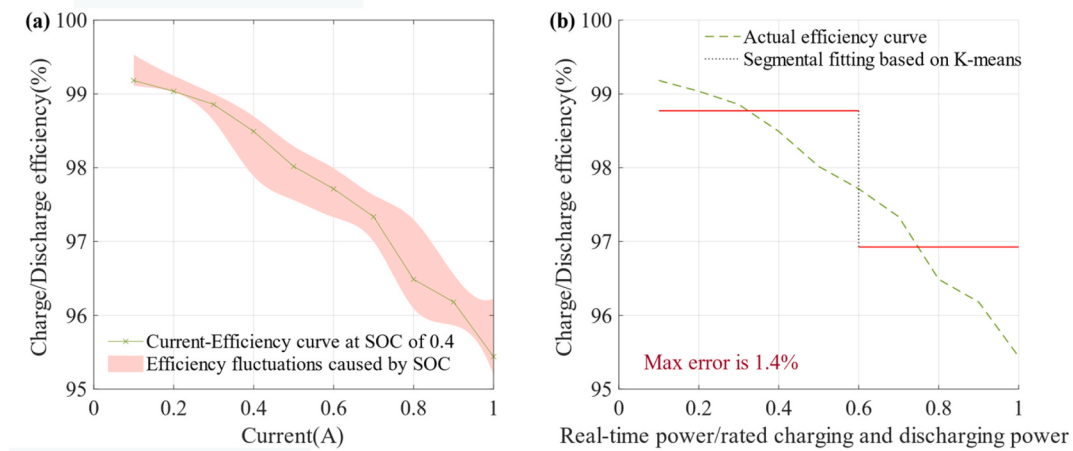


Fig. 6. Dynamic charging/discharging efficiency of electric energy storage.

value.

(ii) Self-discharge loss: the tanks' external surface constantly dissipates heat to the surrounding air. This part of the heat loss is calculated as the self-discharge rate, which mainly depends on the equipment parameters, the real-time temperature of the working mass, the ambient temperature, etc. As shown in the following equations. The self-discharge rate decreases non-linearly as more heat is stored, as shown in Fig. 7a.

In summary, the refined model of thermal storage is displayed in Eqs. (38–45).

$$S_t^{\text{TS}} = S_{t-1}^{\text{TS}} - E_t^{\text{TS}} + (H_{t-1}^{\text{TS},c} \eta^{\text{TS},c} - H_{t-1}^{\text{TS},d} / \eta^{\text{TS},d}) \quad (38)$$

$$E_t^{\text{TS}} = N^{\text{TS}} h^{\text{TS}} A^{\text{TS}} (T_t^{\text{TS}} - T_{\text{ae}}) \quad (39)$$

$$T_t^{\text{TS}} = T_{\min}^{\text{TS}} + S_t^{\text{TS}} (T_{\max}^{\text{TS}} - T_{\min}^{\text{TS}}) / W^{\text{TS}} \quad (40)$$

$$W^{\text{TS}} = N^{\text{TS}} d^{\text{TS}} \partial^{\text{TS}} v^{\text{TS}} (T_{\max}^{\text{TS}} - T_{\min}^{\text{TS}}) \quad (41)$$

$$S_{\min}^{\text{TS}} \leq S_t^{\text{TS}} \leq S_{\max}^{\text{TS}} \quad (42)$$

$$S_0^{\text{TS}} = S_{\text{TS}} \quad (43)$$

$$0 \leq H_t^{\text{TS},c} \leq \tau^{\text{TS}} W^{\text{TS}} \quad (44)$$

$$0 \leq H_t^{\text{TS},d} \leq \tau^{\text{TS}} W^{\text{TS}} \quad (45)$$

where, TS refers to the thermal storage; S_t^{TS} is the storage inventories of the TS at time t ; E_t^{TS} represent heat losses that occur depending on the temperature in the TS ; $H_t^{\text{TS},c}$, $H_t^{\text{TS},d}$ are the charge/discharge power;

$\eta^{\text{TS},c}$ and $\eta^{\text{TS},d}$ are the charging/discharging efficiency; N^{TS} is the number of the installed TS tanks; v^{TS} , A^{TS} and h^{TS} are the volume, tank side area and total convective heat transfer coefficient of a tank; T_t^{TS} , T_{\max}^{TS} and T_{\min}^{TS} refer to the equivalent, maximum and minimum temperature of the TS; W^{TS} is the installed capacity; d^{TS} and ∂^{TS} are the density of the TS medium and its specific heat capacity; τ^{TS} is the power-to-capacity ratio of device.

However, as stated in research [24], the above model suffers from endogenous problems due to the fact that both the number of TS N^{TS} and the real-time energy storage S_t^{TS} are variables in the planning model. Eqs. (38–39) can be deduced as Eq. (46). Then, Eqs. (40–41) can be derived as Eq. (47). They all exhibit significant nonlinear characteristics.

$$S_t^{\text{TS}} = S_{t-1}^{\text{TS}} + N^{\text{TS}} h^{\text{TS}} A^{\text{TS}} (T_{t-1}^{\text{TS}} - T_{\text{ae}}) + (H_{t-1}^{\text{TS},c} \eta^{\text{TS},c} - H_{t-1}^{\text{TS},d} / \eta^{\text{TS},d}) \quad (46)$$

$$T_t^{\text{TS}} = T_{\min}^{\text{TS}} + S_t^{\text{TS}} / (N^{\text{TS}} d^{\text{TS}} \partial^{\text{TS}} v^{\text{TS}}) \quad (47)$$

Taking reference from the Charnes-Cooper variation idea, this paper proposes an equivalent meaning variable $\vartheta_t^{\text{TS}} = T_t^{\text{TS}} N^{\text{TS}}$, which obeys Eq. (48). Then, a linear equivalent model for Eqs. (46–47) is derived as Eqs. (49–50).

$$T_{\min}^{\text{TS}} N^{\text{TS}} \leq \vartheta_t^{\text{TS}} \leq T_{\max}^{\text{TS}} N^{\text{TS}} \quad (48)$$

$$\vartheta_t^{\text{TS}} = T_{\min}^{\text{TS}} N^{\text{TS}} + S_t^{\text{TS}} / (d^{\text{TS}} \partial^{\text{TS}} v^{\text{TS}}) \quad (49)$$

$$S_t^{\text{TS}} = (H_{t-1}^{\text{TS},c} \eta^{\text{TS},c} - H_{t-1}^{\text{TS},d} / \eta^{\text{TS},d}) + S_{t-1}^{\text{TS}} + h^{\text{TS}} A^{\text{TS}} (\vartheta_{t-1}^{\text{TS}} - N^{\text{TS}} T_{\text{ae}}) \quad (50)$$

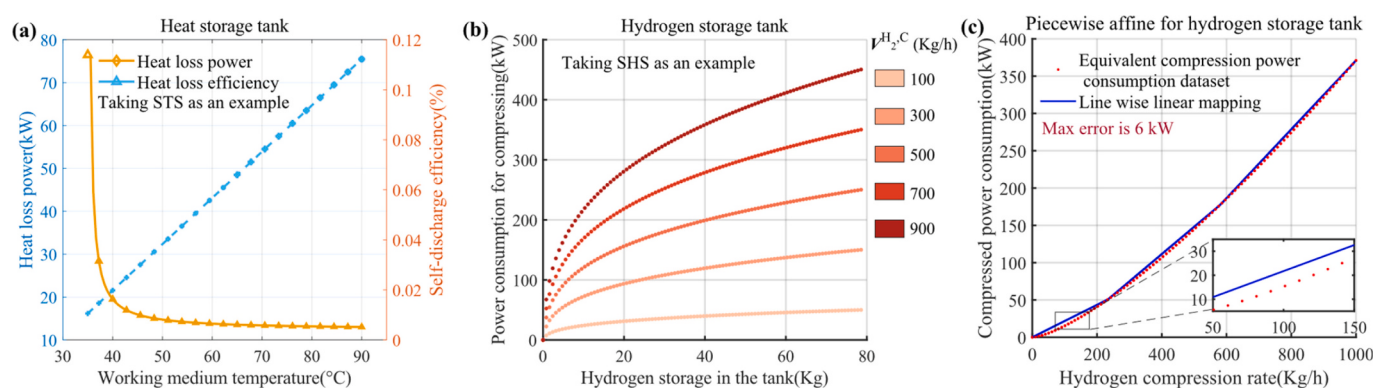


Fig. 7. Differential dynamic characteristics of thermal storage and hydrogen storage.

3.1.3. Refined model of hydrogen energy storage considering compression energy consumption

Hydrogen storage adopts hydrogen storage tank as the energy carrier. Its energy storage model has no unique characteristics, as shown in Eqs. (51–55).

$$S_t^{\text{HS}} = S_{t-1}^{\text{HS}} (1 - \gamma^{\text{HS}}) + (V_{\text{H}_2,t-1}^{\text{HS,c}} \eta^{\text{HS,c}} - V_{\text{H}_2,t-1}^{\text{HS,d}} / \eta^{\text{HS,d}}) \quad (51)$$

$$S_{\min}^{\text{HS}} \leq S_t^{\text{HS}} \leq S_{\max}^{\text{HS}} \quad (52)$$

$$S_0^{\text{HS}} = S_{\text{T}}^{\text{HS}} \quad (53)$$

$$0 \leq V_{\text{H}_2,t}^{\text{HS,c}} \leq \tau^{\text{HS}} W^{\text{HS}} \quad (54)$$

$$0 \leq V_{\text{H}_2,t}^{\text{HS,d}} \leq \tau^{\text{HS}} W^{\text{HS}} \quad (55)$$

where, HS refers to hydrogen storage energy type; S_t^{HS} is the stored hydrogen in time t ; $V_{\text{H}_2,t}^{\text{HS,c}}$ and $V_{\text{H}_2,t}^{\text{HS,d}}$ are the storing/releasing hydrogen rate; $\eta^{\text{HS,c}}$ and $\eta^{\text{HS,d}}$ are the responding efficiency; γ^{HS} refers to the self-discharge rate of HS; τ^{HS} is the power-to-capacity ratio of device; W^{HS} is the installed capacity.

But it will make some unique impact on the system electric power balance, which is characterized by the pressure change process because of hydrogen storage and release. Storing hydrogen requires compression, while releasing is driven by the pressure difference between the tank and the on-board bottle. The compression energy consumption has a multivariate nonlinear relationship with the tank pressure and hydrogen storage rate, as shown in Fig. 7b, which is also calculated as Eqs. (56–58).

$$W^{\text{HS}} = N^{\text{HS}} p_{\text{rated}}^{\text{HS}} v^{\text{HS}} / (GT_{\text{ac}}) \quad (56)$$

$$p_t^{\text{HS}} = S_t^{\text{HS}} p_{\text{rated}}^{\text{HS}} / W^{\text{HS}} \quad (57)$$

$$P_t^{\text{HS}} = \frac{\chi_{\text{H}_2}}{\chi_{\text{H}_2} - 1} \frac{V_{\text{H}_2,t}^{\text{HS,c}} M_{\text{H}_2}}{M_{\text{H}_2}^{\text{v}}} GT_{\text{ac}} \left[\left(\frac{p_t^{\text{HS}}}{p_{\text{ac}}} \right)^{\frac{\chi_{\text{H}_2}-1}{\chi_{\text{H}_2}}} - 1 \right] \frac{1}{3.6 \times 10^9} \quad (58)$$

where, N^{HS} is the installed number of hydrogen tanks; v^{HS} is the volume of hydrogen tank; P_t^{HS} refers to the electrical power consumed by hydrogen compression; p_t^{HS} and $p_{\text{rated}}^{\text{HS}}$ are the equivalent and design pressure of the hydrogen storage tank; χ_{H_2} refers to the thermal insulation index.

Due to the large power generation size of EHTG-IES, its one-hour hydrogen throughput is sufficient to fill multiple hydrogen storage tanks. From the integral median theorem, there must exist a constant value of compression energy for any hydrogen storage rate that makes the total amount of compression energy consumed to fill a single hydrogen storage tank equal (i.e., any of the curves in Fig. 7b can be equated to a line parallel to the x-axis). Therefore, only the storage-rate dependency of the compression energy consumption is considered in the following. This dependency, typically nonlinear, is linearized by piecewise affine for use in an optimization framework (see Fig. 7c).

3.2. Refined model of HESS with multi-timescale

3.2.1. Multi-timescale coupled operation simulation

The synergistic operation of SES and DES provides flexibility to the power system at different time scales. Because of the large number of variables and constraints arising when investigating different technology options, the full-scale optimization is hardly feasible and the time variability during the year is normally simplified [38]. This paper uses clustering approaches to downscale the annual data into multiple typical days to adequately depict the source-load difference on inter-seasonal

time scales [53], and employs these typical days to represent all the natural days of each season. In traditional studies, energy cyclic constraints for energy storage devices are written independently for each typical day, thus decoupling each day from both the previous and next. It is noting that this may result in the problem of limited flexibility of SOC of HESS on long timescale [39].

Then, this study draws on the coupling design days strategy proposed in [38] to expand the time scale of multiple typical days to 8760 h. This strategy allows the system to meet the energy supply/demand balance on a typical-day scale and the SOC constraints for energy storage device on a full-year scale. Taking the case in this study as an example, 4 typical days are selected, resulting in a scale of 4×24 for the power variables of each device. However, the scale of the stored energy variables for each storage device is 365×24 . Each natural day corresponds to a specific typical day. In this case study, the typical days correspond to the seasons, meaning that all natural days within a specific season share the same typical day. The dispatch strategies for the devices remain constant for the same typical day across different natural days, meaning two days of the year described by the same design day must be characterized by the same variation in stored energy. The energy stored in the last hour of each nature day is connected to the energy stored in the first hour of the following nature day. In other words, even though different natural days correspond to the same typical day, the SOC of the energy storage devices are different between these two natural days. The continuous relationship between two days in the same season for HESS is specified in Eq. (59), and the adjacent inter-season energy changes are further formulated in Eq. (60).

$$S_{s,m+1,0}^{\text{ES}} = S_{s,m,24}^{\text{ES}} \quad (59)$$

$$S_{s+1,1,0}^{\text{ES}} = S_{s,m_s,24}^{\text{ES}} \quad (60)$$

where, ES refers to the type of energy storage; $S_{s,m,t}^{\text{ES}}$ refers to the stored energy of ES at time t of m -th nature day in season (typical day) s ; m_s refers to the total number of nature days corresponding to season (typical-day) s .

Thus far, the initial-end constraint of HESS at the SOC within a typical day has been replaced with an initial-end constraint within the planning year. Finally, this study draws on the intra-day and inter-day state superposition strategy proposed in [39] to describe the superposition of interday and intraday states and improve the efficiency of the abovementioned model. Eqs. (59–60) are derived as Eqs. (61–62), which directly extrapolates the ending state by combining the change trend and the initial state, removes the stored energy variable of the intermediate natural days within each single season, and greatly improves the optimization efficiency.

$$S_{s,m+1,0}^{\text{ES}} = S_{s,m,0}^{\text{ES}} (1 - \gamma^{\text{ES}})^{24} + \sum_{t=1}^{24} \left[(P_{s,t-1}^{\text{ES,c}} \eta^{\text{ES,c}} - P_{s,t-1}^{\text{ES,d}} \eta^{\text{ES,d}}) (1 - \gamma^{\text{ES}})^{24-t} \right] \quad (61)$$

$$S_{s+1,1,0}^{\text{ES}} = S_{s,1,0}^{\text{ES}} (1 - \gamma^{\text{ES}})^{24 m_s} + \sum_{m=1}^{m_s} \left\{ (1 - \gamma^{\text{ES}})^{m_s - m} \sum_{t=1}^{24} \left[(P_{s,t-1}^{\text{ES,c}} \eta^{\text{ES,c}} - P_{s,t-1}^{\text{ES,d}} \eta^{\text{ES,d}}) (1 - \gamma^{\text{ES}})^{24-t} \right] \right\} \quad (62)$$

where, $P_{s,t}^{\text{ES,c}}$ and $P_{s,t}^{\text{ES,d}}$ are the charging/discharging power at time t of each nature day in season (typical day) s .

3.2.2. Refined models of energy storage with differential regulation timing characteristics

The frequency of storage/release behavior is a crucial difference between DES and SES, where the storage/release state of DES can vary

within hours, whereas the storage/release behavior of SES is usually measured in months/seasons. Therefore, it is essential to model the difference between them to address this point. Given that the minimum time interval for the optimization process is one hour, DES can be directly simulated by the refined model with dynamic multi-energy characteristics. SES is assumed to have only one storage/release state in each season, determined by intra-seasonal supply and demand. Therefore, SES must add a seasonal net output constraint to the refined model with dynamic multi-energy characteristics, as follows:

$$(\varepsilon_s^{\text{SES}} - 1)\tau^{\text{SES}} W^{\text{SES}} \leq P_{s,t}^{\text{SES}} \leq \varepsilon_s^{\text{SES}} \tau^{\text{SES}} W^{\text{SES}} \quad (63)$$

$$P_{s,t}^{\text{SES}} = P_{s,t}^{\text{SES,c}} - P_{s,t}^{\text{SES,d}} \quad (64)$$

where, $P_{s,t}^{\text{SES}}$ is the net energy release power of the device at time t of each nature day in season s ; $\varepsilon_s^{\text{SES}}$ is the energy flow identifier of the device in typical day s , as a Boolean variable; $P_{s,t}^{\text{SES,c}}$ and $P_{s,t}^{\text{SES,d}}$ are the charging/discharging power of SES.

However, the above equation is a non-linear constraint and needs to be linearized. Functionally, it is split into constraints on positive and negative, and size respectively, as shown in Eqs. (65–66). Eq. (66) is implicitly included in Eq. (64), so only Eq. (65) needs to be retained.

$$(\varepsilon_s^{\text{SES}} - 1)M \leq P_{s,t}^{\text{SES}} \leq \varepsilon_s^{\text{SES}} M \quad (65)$$

$$-\tau^{\text{SES}} W^{\text{SES}} \leq P_{s,t}^{\text{SES}} \leq \tau^{\text{SES}} W^{\text{SES}} \quad (66)$$

where, M is an extremely large positive number and the strategy for taking values is given in [54].

4. Co-optimization configuration method for EHTG-IES with HESS

4.1. Objective function

The costs for proposed EHTG-IES include acquisition costs, operating costs, fuel costs, start/stop costs, and carbon taxes, which are spread evenly over an annuity. Thus, this paper adopts Total Annual Cost (TAC) as the minimized object.

$$f = \min (C_{\text{ic}} + C_{\text{omc}} + C_{\text{fc}} + C_{\text{sc}} + C_{\text{cec}}) \quad (67)$$

$$C_{\text{ic}} = \sum_i^{N_E} k_{\text{ic}}^i W^i \rho (1 + \rho)^{L^i} / [(1 + \rho)^{L^i} - 1] \quad (68)$$

$$C_{\text{omc}} = \sum_i^{N_E} \left(k_{\text{fix}}^i W^i + k_{\text{var}}^i \sum_s \sum_m \sum_t P_{s,t}^i \right) \quad (69)$$

$$C_{\text{fc}} = k_{\text{gas}} \sum_s \sum_m \sum_t (V_{\text{gas},s,t}^{\text{CHP}} - V_{\text{gas},s,t}^{\text{ME}}) \quad (70)$$

$$C_{\text{sc}} = \sum_s \sum_m \sum_t (y_{s,t}^{\text{CHP}} S_{\text{on}}^{\text{CHP}} + z_{s,t}^{\text{CHP}} S_{\text{off}}^{\text{CHP}}) \quad (71)$$

$$C_{\text{cec}} = k_c \sum_s \sum_m \sum_t M_{\text{CO}_2}^{\text{a}} (V_{\text{gas},s,t}^{\text{CHP}} - V_{\text{gas},s,t}^{\text{ME}}) / M_{\text{CH}_4}^{\text{v}} \quad (72)$$

where, k_{ic}^i , k_{fix}^i , k_{var}^i are the acquisition cost, annual fixed cost and O&M cost of equipment i , respectively; L^i is the service life; N_E refers to the set of equipment; ρ refers to the inflation rate; W^i is the installed capacity; $S_{\text{on}}^{\text{CHP}}$ and $S_{\text{off}}^{\text{CHP}}$ are the start-up and shutdown cost of CHP; k_{gas} and k_c are the gas price and carbon tax.

4.2. Model constraints

1) Internal constraints in the energy hub.

Energy hub coupling units mainly consist of CHP, PEMFC, AWE, ME, etc. Its internal constraints mainly include output, ramp, start/stop constraints, etc. As shown in Eqs. (1–66).

2) Available resource constraints.

Subject to local conditions, the system is bounded by capacity, site, and renewable energy consumption constraints, which can be summarized in Eqs. (73–75).

$$W^i \leq W_{\max}^i \quad (73)$$

$$N^i \leq N_{\max}^i \quad (74)$$

$$P_{RP}^{\text{consumption}} \leq P_{RP}^{\text{produce}} = W^i O_{\text{unit}}^i |_{i=\text{PV,WT}} \quad (75)$$

where, W_{\max}^i and N_{\max}^i are the maximum installable capacity and the maximum installable number of equipment i , and are depending on the site area and the government regulations; P_{RP}^{produce} is the maximum real-time power generation from renewable energy sources; $P_{RP}^{\text{consumption}}$ is the true real-time generated power; O_{unit}^i is the normalized output coefficient of WT/PV.

3) Energy balance constraints.

The energy supply and demand in the system are required to be balanced at all times, including electricity, thermal, hydrogen, and natural gas balances, as expressed in Eqs. (76–79).

$$\begin{aligned} & P_{s,t}^{\text{WT,consumption}} + P_{s,t}^{\text{PV,consumption}} + P_{s,t}^{\text{CHP}} + P_{s,t}^{\text{FC}} + P_{s,t}^{\text{TES,d}} \\ & = P_{s,t}^{\text{Load}} + P_{s,t}^{\text{AWE}} + P_{s,t}^{\text{ME}} + P_{s,t}^{\text{TES,c}} + P_{s,t}^{\text{THS}} + P_{s,t}^{\text{SHS}} \end{aligned} \quad (76)$$

$$H_{s,t}^{\text{CHP}} + H_{s,t}^{\text{TTS,d}} + H_{s,t}^{\text{FC}} + H_{s,t}^{\text{AWE}} + H_{s,t}^{\text{ME}} = H_{s,t}^{\text{Load}} + H_{s,t}^{\text{TTS,c}} + H_{s,t}^{\text{STS}} \quad (77)$$

$$V_{\text{H}_2,s,t}^{\text{AWE}} + V_{\text{H}_2,s,t}^{\text{THS,d}} = V_{\text{H}_2,s,t}^{\text{FC}} + V_{\text{H}_2,s,t}^{\text{ME}} + V_{\text{H}_2,s,t}^{\text{TTS,c}} + V_{\text{H}_2,s,t}^{\text{SHS}} \quad (78)$$

$$V_{\text{gas},s,t}^{\text{CHP}} = V_{\text{gas},s,t}^{\text{ME}} + V_{\text{gas},s,t}^{\text{buy}} \quad (79)$$

4.3. Characterization and solution of non-linear features

An accurate description of the interaction characteristics of multiple energy flows and the dynamic non-linear characteristics of the equipment in the mathematical model is the foundation for realistic and reliable planning results. This paper has constructed refined models for various low-carbon technologies, considering the variable operating conditions and the non-linear dynamic operating characteristics. Given the advantages of the piecewise affine method in terms of accuracy, it is used to treat the above-mentioned equipment's performance curves and fuel consumption surfaces in variable operating conditions. The technical features and linearization of the system equipment are shown in Fig. 8. Thus, a linear reduced order model is derived that can be used for MILP optimization while retaining an accurate description of the dynamic characteristics under a variety of operating conditions.

5. Case study and discussion

5.1. Case description and basic data processing

Gansu Province is one of the most favorable regions in China for developing renewable energy. Lanzhou City is one of the province's most renewable resource-rich regions. It has set ambitious energy transition targets for 2025, including new cogeneration projects in Lanzhou New District with a heating area of approximately 12.5 million square meters and a maximum installed capacity of 2×357 MW; and maximum new

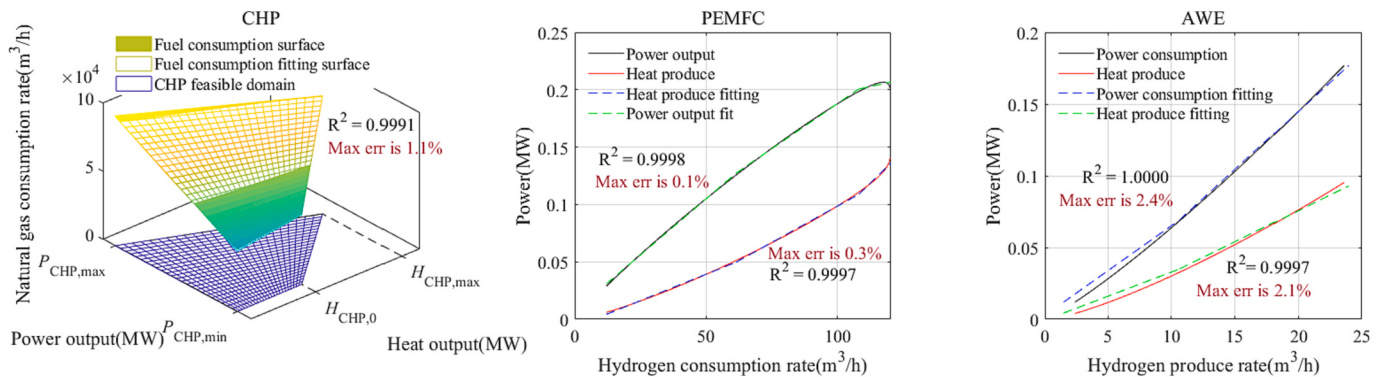


Fig. 8. Linear mapping strategy for refined features of EHTG-IES coupled elements.

ground-based PV installations totaling 2000 MW and WT installations totaling 700 MW in areas such as Shangchuan Town and Heishi Town. This section builds EHTG-IES based on the above project to verify the reliability and superiority of the proposed method. The energy system is assumed to operate in energy hub mode. The weather conditions, energy loads are considered as constant and are not affected by the proposed energy system. The local hourly wind speed, global irradiance, and ambient temperature are shown in Appendix A. The weather data start on January 1st and last for a whole year, and the same data are used for the yearly calculations.

In order to adequately reconstruct the seasonal characteristics of the renewable output series, multiple clustering algorithms are compared, the clustering process and results are shown in Appendix B, and the comparison result is shown in Table 2. The clustering result of K-medoids-Soft-DTW is adopted due to the maximum Silhouette Coefficient and Calinski-Harabasz Index with the minimum Davies-Bouldin Index. The typical-day loads and the normalized output coefficient of WT and PV are displayed in Fig. 9. The detailed technical parameters of the system equipment are shown in the open-source code, and the economic parameters are summarized in Table 3.

It is worth mentioning that the simulation and optimization in this paper are based on the following assumptions: i) Temperature inside the equipment (PEMFC, AWE, ME, TS, HS) is uniform and consistent; ii) Gases in the reaction are ideal gas; iii) The anode reaction gas for PEMFC is hydrogen with a purity of 99% or more, and the cathode reaction gas is air with a nitrogen content of 79% and an oxygen content of 21%; iv) Diffusion and dissolution behaviors of the gases are not taken into account (PEMFC, AWE, ME, HS); v) The reactants, such as hydrogen, are completely reacted; vi) The level of the technology is considered to be not greatly breakthrough in the project planning period.

5.2. Simulation results and further discussion

5.2.1. Simulation results analysis

In order to validate the feasibility and effectiveness of the framed

EHTG-IES optimal configuration method and to explore the advantages of the proposed refined HESS model in terms of DES and SES synergistic planning and the complementary benefits of various novel low-carbon technologies, optimal dispatching was carried out under off-grid conditions in this section.

Fig. 10 demonstrates the system energy supply and demand. Obviously, the energy supply and demand are balanced within each day and the equipment constraints are satisfied, so the feasibility of the model has been guaranteed. Fig. 11 presents the SOC variation of HESS during the whole planning year. It is evident that DES can change the charge/discharge status frequently within the same season, while SES cannot, which is consistent with the model description. Thus, the model's validity is guaranteed. Notably, different from the conventional studies, the SOC at the end of the season is often different from that at the beginning, which precisely reflects the inter-seasonal energy dispatch effect. Additionally, the seasonal variation of storage inventories reveals that DES also shows some seasonal energy transport effect, which is consistent with the results of research [38].

5.2.2. The benefits assessment of refined models

In order to assess the energy use and low-carbon economic benefits of the proposed EHTG-IES with refined modeling, the 4 modeling schemes detailed in Table 4 are investigated.

The capacity of the equipment for each scenario is shown in Table 5. TAC, Annual Carbon Emissions (ACE), Renewable Energy Consumption Rate (RECR), Renewable Energy Penetration Rate (REPR), and Effective Utilization Rate of Production Capacity (EURPC) are adopted as evaluation indicators in this study to assess the economic and low-carbon performance of the EHTG-IES. Their detailed calculations are summarized in Appendix C. Fig. 12 presents the indicators performances of each scheme.

The comparison between S1 and S2 shows that: i) The flexible operating conditions of CHP can significantly promote the wind and solar power real-time consumption, reduce the dependence of the system on energy storage equipment, and make the total system cost decrease by 0.96%, RECR and EURPC increase by 3.58% and 3.81%, respectively. ii) However, the performances of ACE and REPR become worse due to the frequent utilise of CHP.

By comparing S2 and S3, it is evident that: i) The proposed refined modeling approach slightly increases the utilization of the EHC subsystem, thus reducing its redundant acquisition and improving the economics of EHTG-IES; ii) The innovative use of EHC waste heat enhances multi-stage energy utilization. It saves STS allocation, resulting in a decrease in ACE and a modest increase in REPR and EURPC.

Comparing S3 and S4, this paper found that: i) The refined model of HESS makes the model more relevant to reality. Electric energy storage has different efficiency in variable current, the self-attenuation rate of thermal storage decreases with increasing real-time temperature, and

Table 2
Optimal selection of clustering algorithm for reconstructing source load features.

	K-means	Mini Batch K-means	K-medoid-DBA-DTW	K-medoid-Soft-DTW
Silhouette Coefficient	0.321	0.3209	0.1247	0.4821
Calinski-Harabasz Index	99.13	99.44	42.26	123.44
Davies-Bouldin Index	1.52	1.53	2.61	1.23

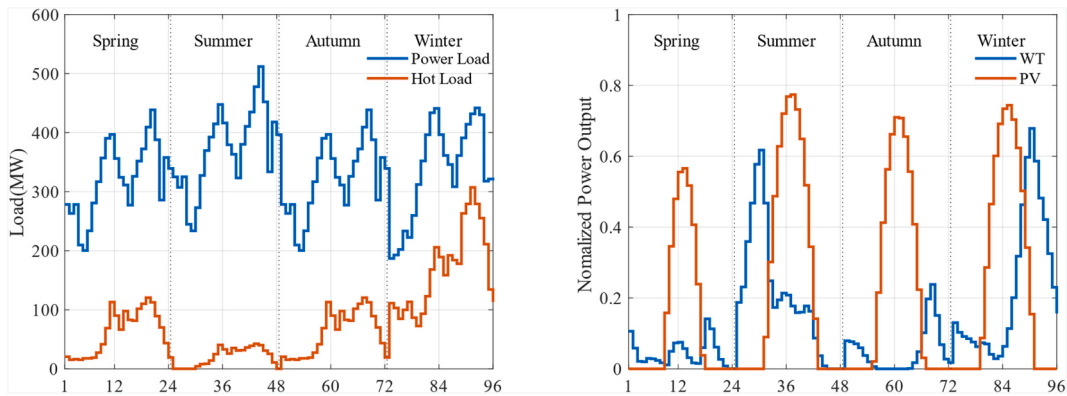


Fig. 9. Typical loads and normalized output coefficient of WT and PV.

Table 3

The economic parameters of EHTG-IES devices [1,55,56].

Equipment	PV	WT	CHP	ME	AWE	PEMFC	DEES	DTS	DHS	STS	SHS
k_{ic} (\$/kW)	710	1400	2067	1750	1490.3	100	52.16	26.08	15	0.53	0.91
k_{fix} (\$/kW)	29.56	40	20	10	0	5	0	0	0	0	0
k_{var} (\$/MW·h)	0.012	0.017	30	0	10	0	10	10	10	5.3	10
L (Year)	25	25	20	25	30	10	10	25	25	25	20

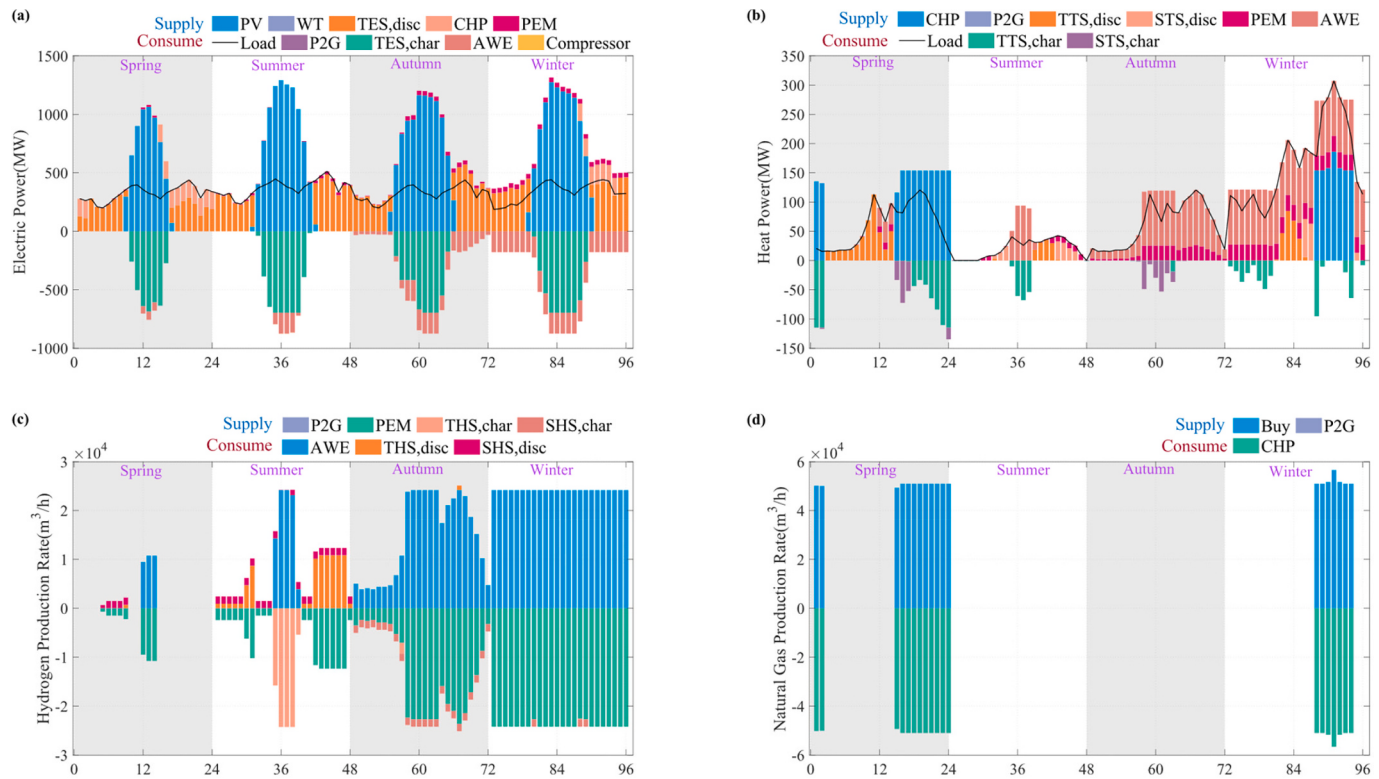


Fig. 10. Energy supply and demand of EHTG-IES in the typical days.

the power of compressors varies with the change of hydrogen storage rate. These are a complete representation of the dynamic behavior of energy storage devices for different energy types as described in Section 3.1, and all these fine features have been verified in the existing literature to be more relevant to reality; ii) The refined use of electric and thermal energy storage makes the system energy storage more efficient,

significantly reduces the capacity of secondary energy conversion equipment such as PEMFC and AWE, and increases the capacity of electric and thermal energy storage, while hydrogen storage brings additional electrical losses, so the system hydrogen storage capacity decreases while the capacity of power generation equipment increases; iii) The refined model of HESS has totally reduced TAC by 2.04% and

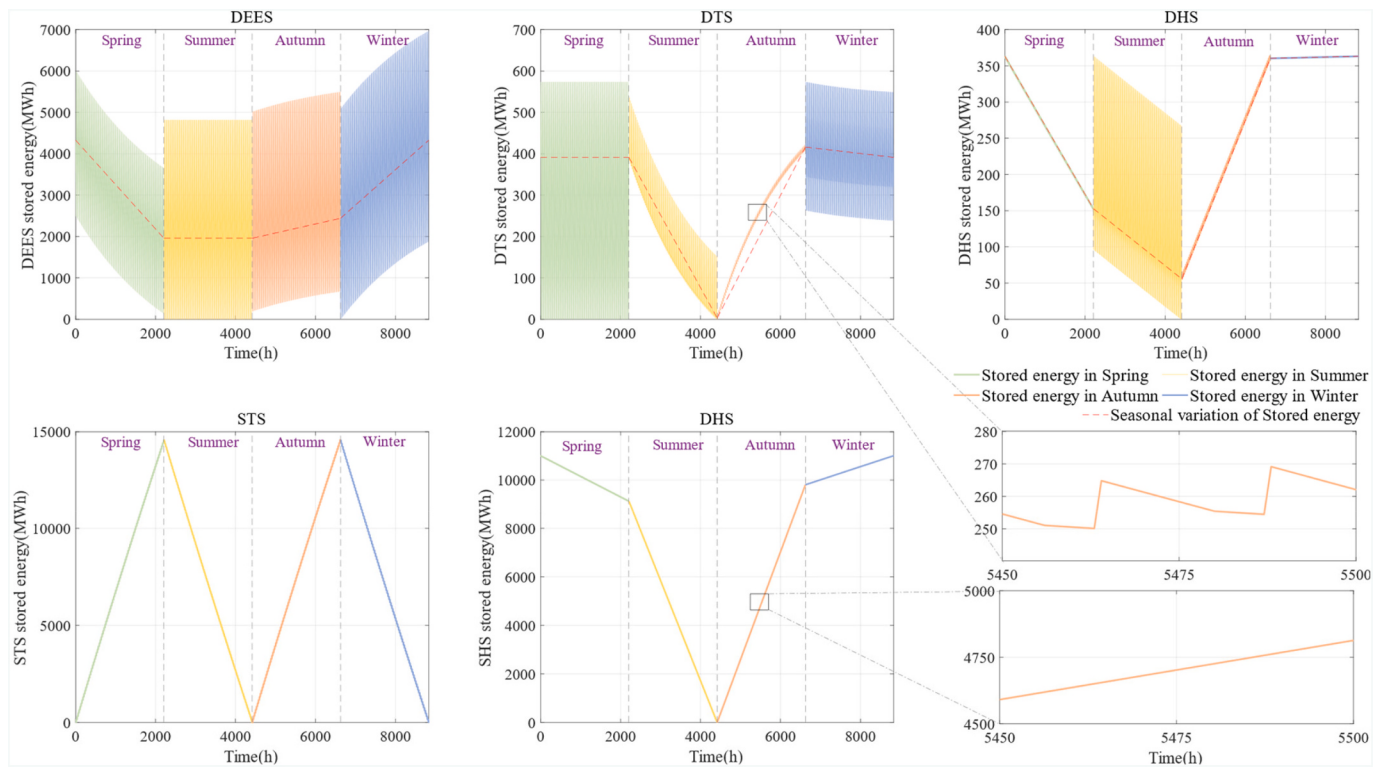


Fig. 11. Time-varying storage inventories of each energy storage device in 8760 h.

Table 4

The comparison modeling schemes setting.

Schemes	CHP	EHC	HESS
S1	Back pressure only	Fixed energy efficiency	Unified model
S2	Refined model	Fixed energy efficiency	Unified model
S3	Refined model	Refined model	Unified model
S4	Refined model	Refined model	Refined model

Note: The charge/discharge efficiency and self-loss rate of the unified model are taken as the integral mean-value of the corresponding dynamic curves. More details are shown in Appendix D.

ACE by 41.11% while simultaneously making the system more dependent on energy storage devices to ensure the balance between supply and demand rather than the real-time generation, so EUPRC has dropped slightly.

In summary, compared to traditional modeling schemes (S1), the refined model proposed in this paper allows EHTG-IES to reduce system costs by 3.18% and carbon emissions by 5.05% at an extremely high REPR.

Table 5

Optimal capacity configuration for each modeling scheme.

	Energy conversion equipment capacity (MW)						Energy storage equipment capacity (MWh)				
	WT	PV	CHP	PEMFC	AWE	ME	DEES	DTS	DHS	STS	SHS
S1	0	1937.6	357	64.7	228.2	0	6966.2	356.1	475.0	13,113.9	1000.8
S2	0	1673.0	357	82.0	252.1	0	5575.0	137.4	502.8	2914.2	2001.7
S3	0	1688.4	357	76.3	244.8	0	5576.0	137.2	456.3	1457.1	2001.7
S4	0	1877.8	357	41.6	178.7	0	6964.0	573.5	363.3	14,571.3	11,009.2

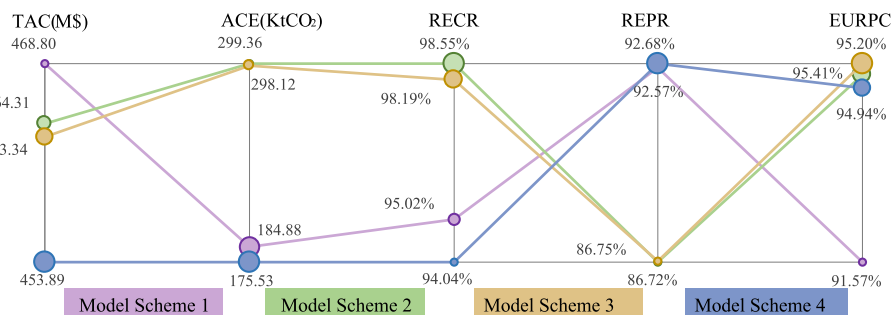


Fig. 12. Comparison of economic and low-carbon indicators for different modeling schemes.

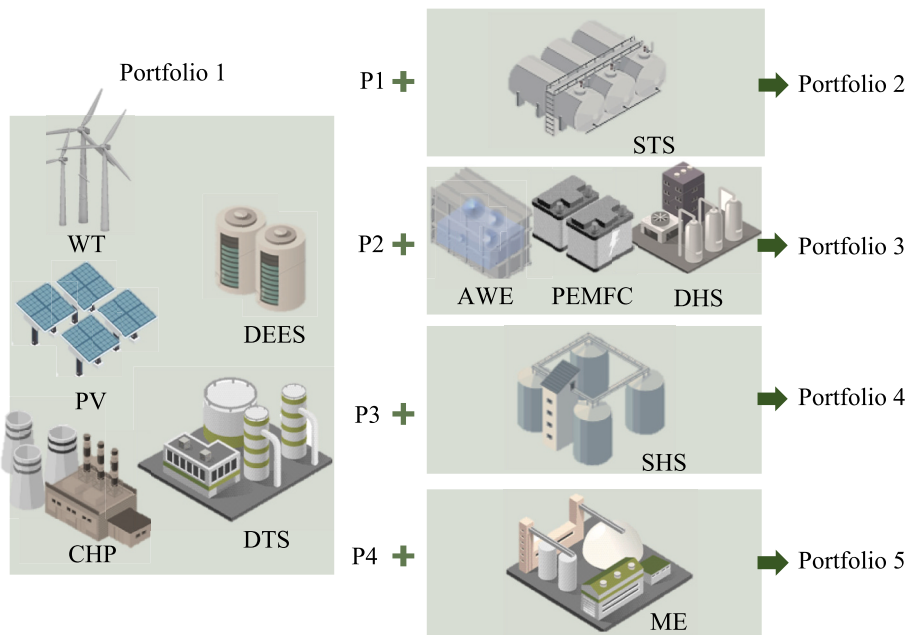


Fig. 13. System composition of each technology portfolio.

Table 6

The optimal capacity configuration of each portfolio.

	Energy conversion equipment capacity (MW)						Energy storage equipment capacity (MWh)				
	WT	PV	CHP	PEMFC	AWE	ME	DEES	DTS	DHS	STS	SHS
P1	0	1200.2	357	0	0	0	3548.6	1138.7	0	0	0
P2	0	1215.2	357	0	0	0	3633.6	947.9	0	14,571.3	0
P3	0	1900.7	357	41.5	178.3	0	7031.6	506.9	363.3	14,571.3	0
P4	0	1877.8	357	41.6	178.7	0	6964.0	573.5	363.3	14,571.3	11,009.2
P5	0	1877.8	357	41.6	178.7	0	6964.0	573.5	363.3	14,571.3	11,009.2

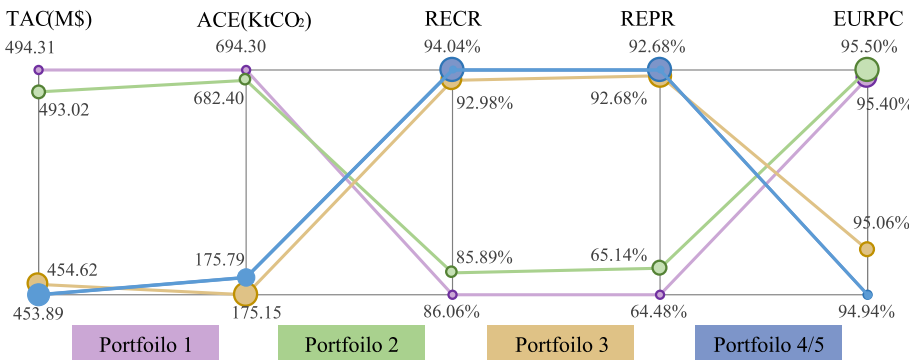


Fig. 14. Key metrics performance for each technology portfolio.

5.2.3. Discussion of the synergistic and complementary benefits of multiple low-carbon technologies

To investigate the synergistic interaction potential of multi-energy flows within EHTG-IES and to examine the techno-economics of different energy subsystems, five technology portfolios were set up for analysis. The detailed setting is presented in Fig. 13. Table 6 displays the optimal capacity configuration results, and Fig. 14 demonstrates the performances of key indicators.

By comparing P2 and P1, we found that: By enabling low-cost inter-

seasonal utilization of surplus heat, STS technology effectively decouples the CHP thermoelectric output and enhances system flexibility, which expands the scope for increased renewable energy consumption while relieving the reliance on TES and TTS, and finally leads to an TAC reduction of 0.26% and a decrease in ACE by 1.71%.

The comparison between P3 and P2 shows that: i) The EHC subsystem provides more alternative heating and energy storage options for the system, significantly optimizing the system supply strategy. As shown in Fig. 15, EHC subsystem provides a continuous heat supply in

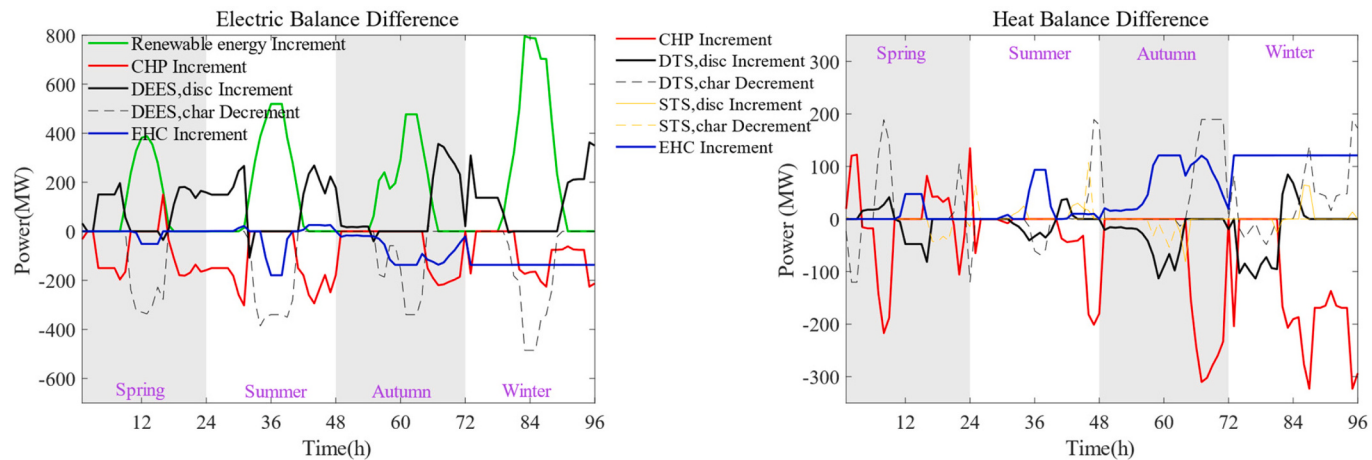


Fig. 15. The difference of energy flow balance between P3 and P2.

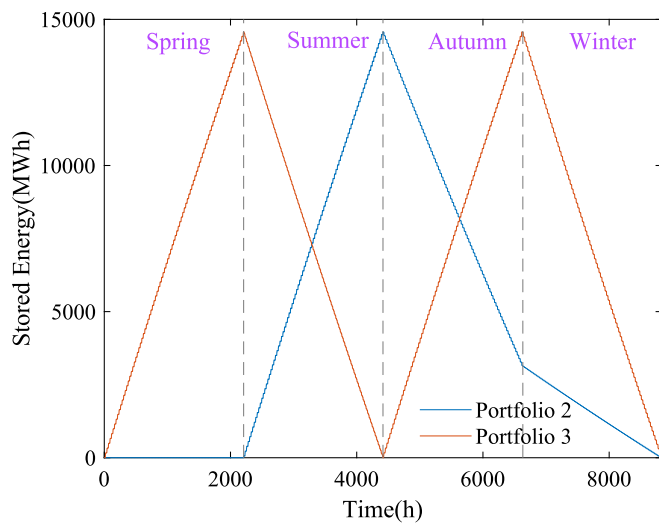


Fig. 16. The 8760 h SOC of STS in P3 and P2.

autumn and winter, resulting in the load on TTS and CHP dropping steeply. The system's renewable energy consumption ability has been improved; ii) The seasonal energy carrying of STS is improved by one time (shown in Fig. 16), and its seasonal energy storage potential is more

fully exploited; iii) The introduction of EHC led to a significant increase in RECP and REPR, and a reduction in TAC and ACE of 7.79% and 74.33%, respectively, compared to P2.

Comparing P3 and P4, it is evident that: i) After the adoption of SHS, the inter-seasonal energy storage role of hydrogen is further exploited, and the renewable generation peaks that are difficult to be consumed can be utilized in-depth, which makes the flexibility of CHP expand and the heating effectiveness of CHP be given full play; ii) However, although SHS can achieve inter-seasonal energy storage at a meager cost, its adoption can only reduce the cost by 0.16%, and the utilization of CHP is synergistically enhanced due to the promotion benefit of SHS on WT and PV peak consumption, thus leading to an increase in carbon emission by 0.37% compared to P3. Therefore, the investment potential of SHS is low due to the fact that THS is already efficient in performing most of the seasonal hydrogen storage with higher flexibility.

Analysis of the capacity configuration results for P4 and P5 reveals that: ME is not utilized, indicating the poor technical economics of Power-to-Gas system at the current carbon tax and natural gas price.

In summary, the synergistic interaction potential between multiple low-carbon technologies in EHTG-IES is mainly manifested in: i) HESS can considerably enhance the flexibility of CHP units and significantly promote renewable energy consumption; ii) EHC subsystem expands the system supply and storage pathways, helps CHP thermoelectric decoupling, and realize a deeper utilization of STS; iii) THS and SHS have more overlapping roles, so there is insufficient investment driving force for SHS. iv) The synergy between ME and CHP is not obvious under the current natural gas and carbon tax prices.

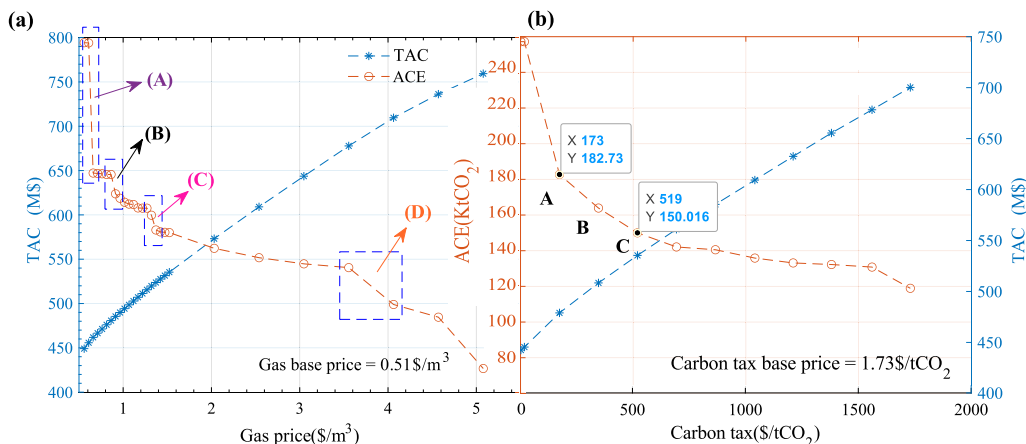


Fig. 17. The sensitivity analysis of TAC and ACE to the price of natural gas and carbon tax.

5.2.4. Sensitivity analysis for low-carbon target

The reason that ME is not employed under the existing conditions and optimization objectives is that the system has insufficient attention to carbon emission reduction targets. However, the ‘dual carbon target’ requires the power system put more attention on carbon reduction. In this regard, this section implements sensitivity analysis by varying the key influencing factors, such as natural gas price and carbon tax, with a view to investigate in depth the changes in the complementary effect of various low-carbon technologies under different low-carbon target concerns and the regulatory effects of each factor on carbon emission reduction. The sensitivity analysis of natural gas and carbon tax price is implemented. The performance variations of ACE and TAC for EHTG-IES are illustrated in Fig. 17. The optimal capacity configuration under different low-carbon target concerns is given in Appendix E.

Based on Fig. 17-a and Appendix E, the synergistic benefits of multiple technologies under different carbon reduction target concerns are explored as follows: i) As the price of natural gas and carbon tax increases, that is, the concern about the carbon reduction target increases, the TAC also increased nearly linearly, with the linear fit indicator R^2 as high as 0.9941 and 0.9954, respectively; ii) As illustrated in Fig. 17-a-(A), once the natural gas price reached 0.66\$/m³, the capacity of PV and DEES increased greatly while DTS decreased abruptly. The substitution effect of PV and DEES on DTS appeared, making ACE decrease significantly by up to 28.5% while TAC increased slightly; iii) When the natural gas price reached 0.914\$/m³ (Fig. 17-a-(B)), ME was acquired for the first time. The synergistic benefits of ME and CHP emerged, with a relatively large decrease in ACE by 5.97%, compared to when the price at 0.86\$/m³; iv) In Fig. 17-a-(C), the natural gas price reached 1.32 \$/m³, the substitution effect of PV and DEES to DTS reached the maximum, and the substitution effect of PV and DTS to THS began to appear. Therefore, the capacity of DESS no longer increased while DTS became more and THS increased, making ACE decrease by 2.44% compared to when the price at 1.27\$/m³; v) In Fig. 17-a-(D), the price reached 4.06\$/m³, and the substitution effect of WT on STS and THS is significantly highlighted. The installed capacity of WT was 229.7 MW, while the capacity of STS and THS decayed remarkably, allowing a significant reduction in ACE.

Furthermore, by comparing Fig. 17a and Fig. 17b, we analyzed the regulatory effects of each factor on carbon emission reduction as follows: i) The ACE total decreases by 28.96% when the carbon tax price multiplies 100 times (Fig. 17-b-A), while the natural gas price only needs to be expanded by approximately one times the original price to accomplish the same result. When the carbon tax increased by a factor of 200 (Fig. 17-b-B), ME was acquired for the first time, while the gas price just needed to be 1.9 times. Similarly, after a 300-times tax increase

(Fig. 17- a-C), ACE is reduced by 36.27%, while the gas price is expanded by approximately only 2.6 times; ii) The ACE of EHTG-IES is sensitive to the gas price based on the fuel consumption of CHP and insensitive to the carbon tax due to the low price of the current baseline carbon tax. By the way, similar conclusions were drawn in the study [5].

In summary: i) The synergistic complementary and substitution effects of EHTG-IES will change with the increasing emphasis on the carbon reduction target; ii) Raising the natural gas price by 30% will increase TAC by only 4.38% and reduce ACE by 28.62%; iii) The effectiveness of the current carbon tax price in regulating ACE is only about 1 % of the natural gas price due to the low benchmark price.

5.2.5. Influence analysis of source-load endowment on EHTG-IES with HESS

The differences in source-load endowments of various regions therefore contribute to changes in the optimal configuration of EHTG-IES. In the context, the source-load is given as the coefficient curves of renewable energy output and load demand, which have no differences on the same typical day, and the distribution of typical days is the same for the different years of the planning period. To explore the impact of source-load endowments on EHTG-IES with HESS, this section compares and analyzes the system configuration results from 2 aspects: First, the four seasons are used as the start-up seasons respectively for optimization. Second, the season-to-year ratio is adjusted on the basis of the optimal starting season. The time at which the system is put into operation determines the sequence of seasons that the system goes through, i.e., the temporal sequence of source loads faced by the system. The season-to-year ratio determines the duration of seasons. Detailed settings are displayed in Fig. 18.

The equipment capacity configurations for each start-up season are listed in Table 7, the system economic and low-carbon indicators are summarized in Fig. 19.

CHP has insufficient output margin in spring, summer, and autumn, constrained by energy storage capacity, renewable capacity consumption potential, and total load energy demand. In contrast, the renewable generation is low, and the energy demand is high in winter, especially a large amount of thermal energy is needed to meet the heating demand. Therefore, CHP would be fully utilized in winter (as shown in Fig. 20). Additionally, the surplus can be used to compensate for the energy deficit in the rest of the season with the help of SES.

In summary, starting the system in winter will improve the real-time generation consumption, enhance the synergy between CHP and SES, and minimize redundant power generation units. Selecting the best start-up season can further reduce the TAC by 5.04% and improve RECR under the premise of high REPR. Thus, the investor can request the

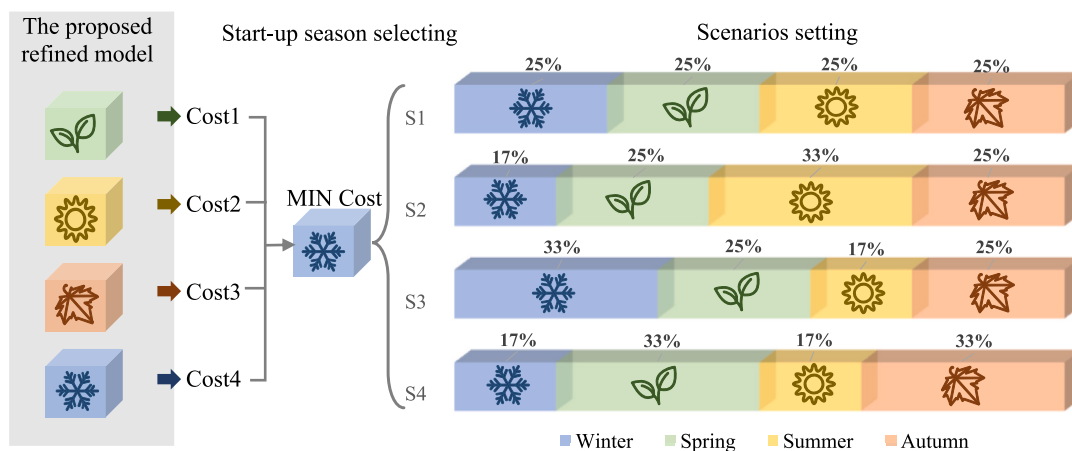
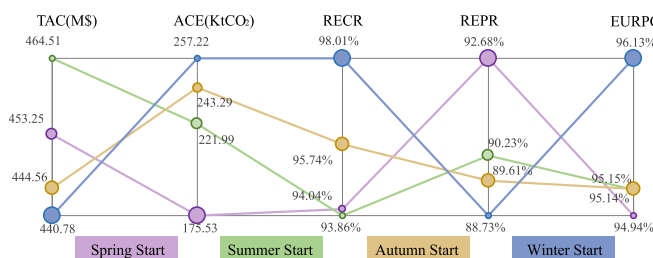


Fig. 18. The analytical process for the effect of source-load endowment.

Table 7

The optimal capacity configuration of each start-up season scenario.

Start-up season	Energy conversion equipment capacity (MW)						Energy storage equipment capacity (MWh)				
	WT	PV	CHP	PEMFC	AWE	ME	TES	TTS	THS	STS	SHS
Spring	0	1877.8	357	41.6	178.7	0	6964.0	573.5	363.3	14,571.3	11,009.2
Summer	0	1878.3	357	46.9	187.0	0	6814.3	406.9	379.2	14,571.3	9803.8
Autumn	0	1719.8	357	46.2	151.7	0	5990.7	638.1	307.6	14,571.3	0
Winter	0	1638.1	357	44.7	124.0	0	6468.1	506.2	251.9	14,571.3	4205.5

**Fig. 19.** Key metrics performance for each start-up season scenario.

company undertaking the construction to set up an appropriate construction schedule so that the system can be put into operation at the winter.

Subsequently, this paper adjusted the year ratio of each season based on the winter season as the system start-up season. The setting has been shown in Fig. 18. The optimal capacity configuration of EHTG-IES under each year-ratio season scenario is shown in Table 8, and the performance of key indicators is summarized in Fig. 21.

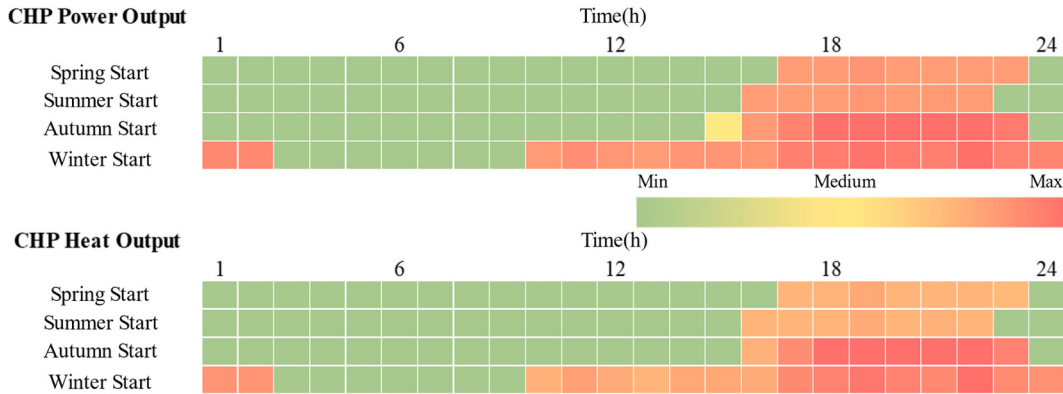
It can be seen that: i) HESS capacity fluctuates significantly with seasonal characteristics, which indicates that both the start-up season and season ratio significantly impact on the diurnal and seasonal energy complementary potential of EHTG-IES; ii) In S2, the system indicators perform best because of the long summer season with sufficient

renewable resources, which ensure the deep utilization of seasonal energy storage effectiveness. In other words, EHTG-IES constructed in areas with short winters and long summers performs better. iii) Different seasonal duration scenarios will cause significant changes in system costs and carbon emissions, with fluctuations of up to 10.28% and 41.58%, respectively.

In summary, the impact of different season setting methods on EHTG-IES mainly lies in: (i) the source-load temporal sequence experienced by EHTG-IES depends on the start-up season, and the CHP generation margin will change significantly; (ii) the total renewable resources and seasonal energy storage potential of EHTG-IES will change significantly with different annual ratios of seasons; (iii) proper planning of EHTG-IES combined with the source-load temporal endowment can significantly reduce the redundant investment in HESS and power generation equipment, and realize the quality and efficiency improvement of EHTG-IES low-carbon economic planning.

6. Conclusion

In order to further explore the complementary mutual benefit potential between different low-carbon technologies of EHTG-IES under multi-energy flow, variable operating conditions, and multi-timescale and to summarize the multi-energy complementary synergistic mechanism from simulation, this paper proposes a refined modeling and co-optimization configuration method for EHTG-IES with HESS, in which the key findings are as follows:

**Fig. 20.** CHP winter output scheduling under different start-up season scenarios.**Table 8**

The optimal capacity configuration of EHTG-IES under different year ratios of seasons.

Season scenario	Energy conversion equipment capacity (MW)						Energy storage equipment capacity (MWh)				
	WT	PV	CHP	PEMFC	AWE	ME	TES	TTS	THS	STS	SHS
S1	0	1638.1	357	44.7	124.0	0	6468.1	506.2	251.9	14,571.3	4205.5
S2	0	1637.9	357	43.0	122.9	0	6553.6	467.2	249.2	14,571.3	5285.8
S3	0	1641.2	357	43.7	125.6	0	6459.2	504.9	254.6	14,571.3	3875.1
S4	0	1642.1	357	46.3	134.0	0	6476.0	471.3	273.1	14,571.3	6964.5

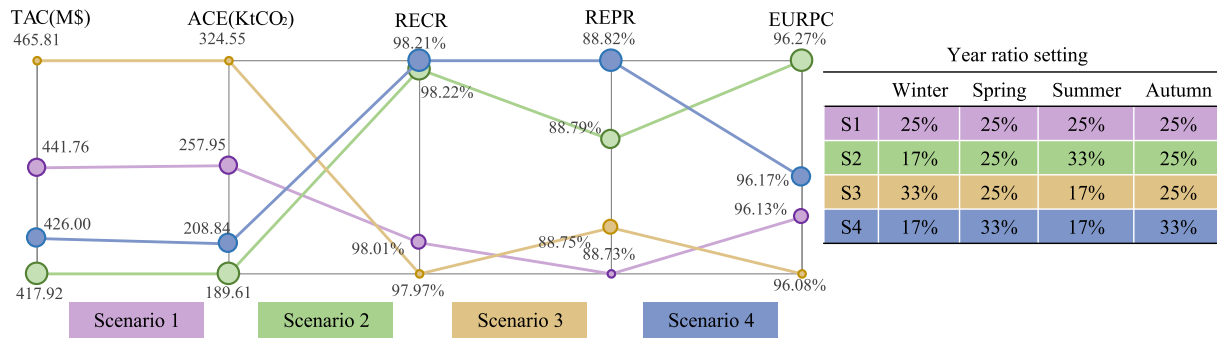


Fig. 21. The key indicators of different year-ratio scenarios.

- 1) A refined model of HESS containing electricity, thermal, and hydrogen multi-energy mediums is constructed to describe the different and dynamic characteristics in the physical and chemical processes of multi-energy storages. Then, as such non-linear models are intractable for the MILP-based optimization of EHTG-IES, different effective linear order-reduction and relaxation strategies are proposed. In particular, this paper solves the endogenous optimization problem of thermal storage mentioned in [24], realizing the tracking of real-time temperature and dynamic self-discharge for thermal storage without deviation.
- 2) Coupling design days method and the intra-day and inter-day state superposition strategies are combined in this paper, efficiently solving the problem of restricted flexibility for SOC on the long timescale. The simulation results indicate that the combination method further enhances the complementary and co-dispatch of heterogeneous energy sources in EHTG-IES and highlights the medium- and long-term energy storage effect of DES.
- 3) EHTG-IES considering the intricate characteristics of the coupling components can fully exploit the complementary and mutually beneficial potential of different low-carbon technologies, reduce the inefficient operation of equipment, and reduce planning cost input by 3.18% and carbon emission by 5.05% under a high-level clean energy penetration rate.
- 4) Different low-carbon technologies have not only significant synergistic and complementary effects but also competitive substitution phenomenon, which cannot be ignored. HESS can significantly improve the flexibility of CHP. EHC contributes to the thermoelectric decoupling of CHP and enables a deeper utilization of STS. However, DHS and SHS play many of the same responsibilities, resulting in insufficient investment drivers for the latter. In addition, the coupling effect between ME and CHP is not noticeable under the existing gas and carbon tax prices.
- 5) The synergistic complementary and substitution effects of low-carbon technologies change with the increasing emphasis on the carbon reduction target. An appropriate increase in the unit cost of carbon emissions allows for a 28.62% decrease in system carbon emission at a cost increase of 4.38%. The stimulative impact of

carbon taxes on carbon reduction in the system is about 1% of the price of natural gas.

- 6) Combining the source-load endowments for EHTG-IES planning can effectively reduce the redundant investment in HESS and generation equipment and realize system quality and efficiency improvements. The source-load temporal sequence experienced by EHTG-IES depends on the start-up season. If the start-up season is adequately selected, it would be conducive to improving the economics of HESS, which could reduce the system investment by up to 5.04%. Additionally, the annual ratios of different seasons exhibit the varying potential of diurnal and seasonal energy complementarity.

CRediT authorship contribution statement

Haoxin Dong: Writing – review & editing, Writing – original draft, Visualization, Validation, Software, Methodology, Investigation, Formal analysis, Data curation, Conceptualization. **Zijing Shan:** Writing – review & editing. **Jianli Zhou:** Validation, Supervision, Methodology. **Chuanbo Xu:** Resources, Funding acquisition. **Wenjun Chen:** Supervision, Resources.

Declaration of Competing Interest

The authors declare that they have no known competing financial interests or personal relationships that could have appeared to influence the work reported in this paper.

Data availability

Data will be made available on request.

Acknowledgment

This research is supported by the National Key Research and Development Program of China [Grant No. 2021YFE0102400], the National Social Science Fund of China [Grant No. 21&ZD133], and Beijing Social Science Fund [Grant No. 22JCC092].

Appendix A

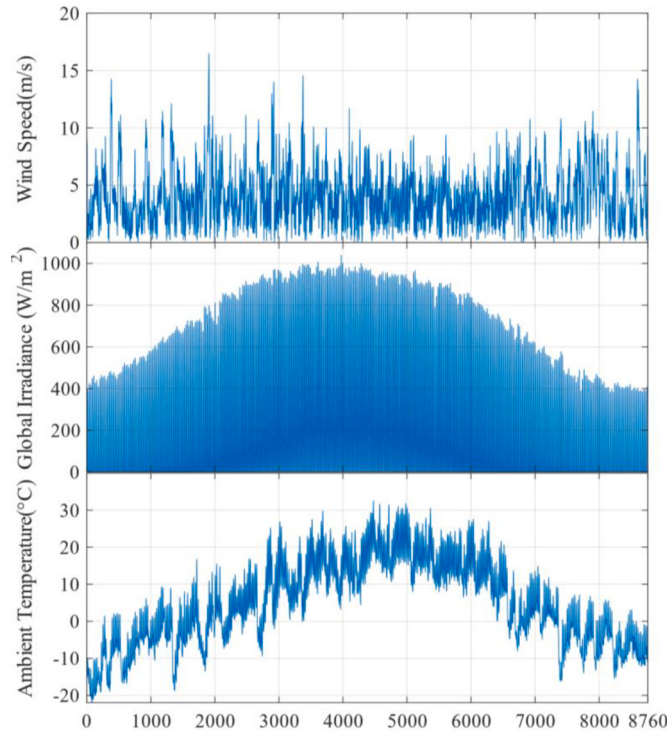


Fig. A1. Annual hourly weather conditions.

Annotation: the data is taken from NASA public data; The data is taken from a certain region in Gansu in 2021.

Appendix B

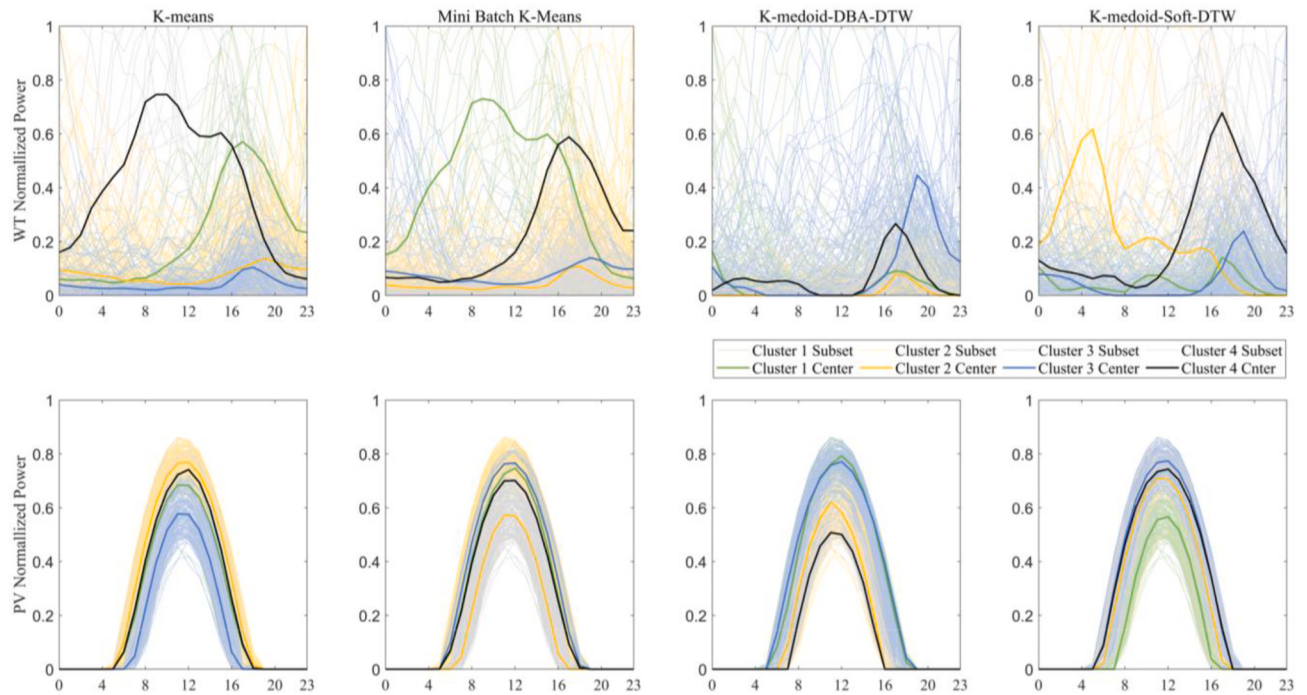


Fig. B1. The clustering results of multi algorithms for reconstructing the features of renewable resource.

Appendix C

The calculation formulas of ACE, RECR, REPR, and EURPC are as follows

$$ACE = \sum_s \sum_m \sum_t M_{q,CO_2} \left(V_{\text{gas } s,t}^{\text{CHP}} - V_{\text{gas } s,t}^{\text{ME}} \right) / M_{\text{gas}}^v \quad (80)$$

$$RECR = \sum_s \sum_m \sum_t P_{RP}^{\text{consumption}} / P_{RP}^{\text{produce}} \quad (81)$$

$$REPR = \sum_s \sum_m \sum_t P_{RP}^{\text{consumption}} / (P_{RP}^{\text{consumption}} + P_{s,t}^{\text{CHP}}) \quad (82)$$

$$EURPC = \sum_s \sum_m \sum_t (P_{s,t}^{\text{Load}} + H_{s,t}^{\text{Load}}) / (P_{s,t}^{\text{WT,consumption}} + P_{s,t}^{\text{PV,consumption}} + P_{s,t}^{\text{CHP}} + H_{s,t}^{\text{CHP}}) \quad (83)$$

Appendix D

Modeling CHP running only at backpressure conditions requires changing Eq. (8) to Eq. (84), and the rest is consistent with the refined model of CHP (Eqs. (7–14))

$$P_t^{\text{CHP}} = K u_t^{\text{CHP}} + c_m H_t^{\text{CHP}} \quad (84)$$

The difference between EHC with refined model and with a fixed energy efficiency model is the linearized approach. The refined model adopts the piecewise affine approximation method (A1), and the fixed energy efficiency model adopts affine approximation method (A2). EHC are cogenerative systems, i.e. they generate electricity/hydrogen and heat at the same time. The following equations express the output power of A1 (Eqs. (85–86)) and A2 (Eqs. (87–88)) [13].

$$P_t^{\text{EHC}} = \alpha_i^P F + \beta_i^P Sx + \gamma_i^P x \quad (85)$$

$$H_t^{\text{EHC}} = \alpha_i^H F + \beta_i^H Sx + \gamma_i^H x \quad (86)$$

$$P_t^{\text{EHC}} = \alpha^P F + \beta^P Sx + \gamma^P x \quad (87)$$

$$H_t^{\text{EHC}} = \alpha^H F + \beta^H Sx + \gamma^H x \quad (88)$$

where, F is the input power of EHC; α, β, γ express the power and size dependencies of the generated electric power/hydrogen production rate, with the index i referring to the i -th affine segment of the A1; P/H are the indices determine the dependencies whether on power (hydrogen) or heat.

The energy storage unified model reflects the commonality of different types of energy storage in terms of energy variation across time. In this model, dynamic characteristics of HESS with different energy medium are ignored. Detailed of the model is as follows:

$$S_{s,m,t}^{\text{ES}} = (P_{s,t-1}^{\text{ES,c}} \eta^{\text{ES,c}} - P_{s,t-1}^{\text{ES,d}} / \eta^{\text{ES,d}}) + (1 - \gamma_{\text{ES}}) S_{s,m,t-1}^{\text{ES}} \quad (89)$$

$$S_{\min}^{\text{ES}} \leq S_{s,m,t}^{\text{ES}} \leq S_{\max}^{\text{ES}} \quad (90)$$

$$S_0^{\text{ES}} = S_T^{\text{ES}} \quad (91)$$

$$0 \leq P_{s,t}^{\text{ES,c}} \leq u_{s,t}^{\text{ES,c}} \tau_{\text{ES}} W^{\text{ES}} \quad (92)$$

$$0 \leq P_{s,t}^{\text{ES,d}} \leq u_{s,t}^{\text{ES,d}} \tau_{\text{ES}} W^{\text{ES}} \quad (93)$$

where, $P_{s,t}^{\text{ES,c}}$ and $P_{s,t}^{\text{ES,d}}$ are the discharge/charge power; $\eta^{\text{ES,c}}$ and $\eta^{\text{ES,d}}$ are the charging/discharging efficiency; γ_{ES} is the self-attenuation rate; S_0^{ES} and S_T^{ES} are the stored energy at the initial and final moments of the optimization cycle; S_{\min}^{ES} and S_{\max}^{ES} are the minimum and maximum of the stored energy for EES.

Appendix E

Table E1

The optimal capacity configuration under different carbon reduction concerns.

Gas Price	Growth rate	WT	PV	CHP	PEMFC	AWE	ME	DEES	DTS	DHS	STS	SHS
0.51	0%	0	1643	357	43	123	0	6524	631	249	14,571	2929
0.56	10%	0	1644	357	43	123	0	6519	630	249	14,571	2830
0.61	20%	0	1644	357	43	123	0	6515	630	249	14,571	2500
0.66	30%	0	1876	357	47	126	0	7485	81	255	14,571	3670

(continued on next page)

Table E1 (continued)

Gas Price	Growth rate	WT	PV	CHP	PEMFC	AWE	ME	DEES	DTS	DHS	STS	SHS
0.71	40%	0	1877	357	48	125	0	7499	79	252	14,571	3197
0.76	50%	0	1878	357	49	125	0	7507	78	252	14,571	2813
0.81	60%	0	1884	357	50	126	0	7442	73	255	14,571	2786
0.86	70%	0	1884	357	50	126	0	7442	73	255	14,571	2786
0.91	80%	0	1892	357	51	127	17	7389	68	286	14,571	2089
0.96	90%	0	1898	357	52	127	20	7351	62	308	14,571	1696
1.02	100%	0	1901	357	51	127	23	7362	64	326	14,571	402
1.07	110%	0	1902	357	50	128	25	7359	65	323	14,571	0
1.12	120%	0	1902	357	50	129	25	7357	66	313	14,571	0
1.17	130%	0	1902	357	49	129	29	7355	66	316	14,571	0
1.22	140%	0	1902	357	49	129	29	7353	66	308	14,571	0
1.27	150%	0	1902	357	49	129	29	7353	66	308	14,571	0
1.32	160%	0	1916	357	42	123	31	7495	187	249	14,571	0
1.37	170%	0	1996	357	36	144	31	6937	584	225	11,657	0
1.42	180%	0	2000	357	38	146	32	6951	580	215	10,200	0
1.47	190%	0	2000	357	38	146	32	6955	580	212	10,200	0
1.52	200%	0	2000	357	38	146	33	6956	580	212	10,200	0
2.03	300%	0	2000	357	38	146	43	7606	558	191	14,571	0
2.54	400%	0	2000	357	31	132	48	8283	395	194	14,571	0
3.05	500%	0	2000	357	33	143	53	8661	325	125	10,200	0
3.56	600%	16	2000	357	34	147	55	8728	302	111	5829	0
4.06	700%	230	2000	357	31	152	73	8873	275	106	0	0
4.57	800%	307	2000	357	32	152	73	9022	211	82	0	0
5.08	900%	700	2000	357	52	225	100	7856	868	66	0	0

References

- [1] Pan G, Gu W, Lu Y, Qiu H, Lu S, Yao S. Optimal planning for electricity-hydrogen integrated energy system considering power to hydrogen and heat and seasonal storage. *IEEE Transact Sustain Energy* 2020;11:2662–76.
- [2] Chen Q, Kuang Z, Liu X, Zhang T. Energy storage to solve the diurnal, weekly, and seasonal mismatch and achieve zero-carbon electricity consumption in buildings. *Appl Energy* 2022;312:118744.
- [3] Milan C, Stadler M, Cardoso G, Mashayekh S. Modeling of non-linear CHP efficiency curves in distributed energy systems. *Appl Energy* 2015;148:334–47.
- [4] Liu Z, Chen Y, Zhuo R, Jia H. Energy storage capacity optimization for autonomy microgrid considering CHP and EV scheduling. *Appl Energy* 2018;210:1113–25.
- [5] Zhou J, Wu Y, Zhong Z, Xu C, Ke Y, Gao J. Modeling and configuration optimization of the natural gas-wind-photovoltaic-hydrogen integrated energy system: a novel deviation satisfaction strategy. *Energy Convers Manag* 2021;243:114340.
- [6] Guo J, Liu Z, Wu X, Wu D, Zhang S, Yang X, et al. Two-layer co-optimization method for a distributed energy system combining multiple energy storages. *Appl Energy* 2022;322:119486.
- [7] Yang J, Zhang N, Cheng Y, Kang C, Xia Q. Modeling the operation mechanism of combined P2G and gas-fired plant with CO₂ recycling. *IEEE Transact Smart Grid* 2019;10:1111–21.
- [8] Candas S, Muschner C, Buchholz S, Bramstoft R, van Ouwerkerk J, Hainsch K, et al. Code exposed: review of five open-source frameworks for modeling renewable energy systems. *Renew Sust Energ Rev* 2022;161:112272.
- [9] Zhou Z, Liu P, Li Z, Pistikopoulos EN, Georgiadis MC. Impacts of equipment off-design characteristics on the optimal design and operation of combined cooling, heating and power systems. In: Karimi IA, Srinivasan R, editors. Computer Aided Chemical Engineering. Elsevier; 2012. p. 990–4.
- [10] Li G, Zhang R, Jiang T, Chen H, Bai L, Cui H, et al. Optimal dispatch strategy for integrated energy systems with CCHP and wind power. *Appl Energy* 2017;192:408–19.
- [11] Ebrahimi M, Derakhshan E. Design and evaluation of a micro combined cooling, heating, and power system based on polymer exchange membrane fuel cell and thermoelectric cooler. *Energy Convers Manag* 2018;171:507–17.
- [12] Li J, Lin J, Song Y, Xing X, Fu C. Operation optimization of power to hydrogen and heat (P2HH) in ADN coordinated with the district heating network. *IEEE Transact Sustain Energy* 2019;10:1672–83.
- [13] Gabrielli P, Gazzani M, Mazzotti M. Electrochemical conversion technologies for optimal design of decentralized multi-energy systems: modeling framework and technology assessment. *Appl Energy* 2018;221:557–75.
- [14] Schiebahn S, Grube T, Robinius M, Tietze V, Kumar B, Stolten D. Power to gas: technological overview, systems analysis and economic assessment for a case study in Germany. *Int J Hydrg Energy* 2015;40:4285–94.
- [15] Burrin D, Roy S, Roskilly AP, Smallbone A. A combined heat and green hydrogen (CHH) generator integrated with a heat network. *Energy Convers Manag* 2021;246:114686.
- [16] Le TS, Nguyen TN, Bui D-K, Ngo TD. Optimal sizing of renewable energy storage: a techno-economic analysis of hydrogen, battery and hybrid systems considering degradation and seasonal storage. *Appl Energy* 2023;336:120817.
- [17] Gabrielli P, Poluzzi A, Kramer GJ, Spiers C, Mazzotti M, Gazzani M. Seasonal energy storage for zero-emissions multi-energy systems via underground hydrogen storage. *Renew Sust Energ Rev* 2020;121:109629.
- [18] Evins R, Orehoung K, Dorer V, Carmeliet J. New formulations of the ‘energy hub’ model to address operational constraints. *Energy*. 2014;73:387–98.
- [19] Jia K, Liu C, Li S, Jiang D. Modeling and optimization of a hybrid renewable energy system integrated with gas turbine and energy storage. *Energy Convers Manag* 2023;279:116763.
- [20] Petkov I, Gabrielli P, Spokaite M. The impact of urban district composition on storage technology reliance: trade-offs between thermal storage, batteries, and power-to-hydrogen. *Energy*. 2021;224:120102.
- [21] Bahllawan H, Losi E, Manservigi L, Morini M, Pinelli M, Spina PR, et al. Optimization of a renewable energy plant with seasonal energy storage for the transition towards 100% renewable energy supply. *Renew Energy* 2022;198:1296–306.
- [22] Allan J, Croce L, Dott R, Georges G, Heer P. Calculating the heat loss coefficients for performance modelling of seasonal ice thermal storage. *J Energy Stor* 2022;52:104528.
- [23] Luo Y, Cui De Hu L, Ochs F, Tosatto A, Xu G, et al. Semi-analytical modeling of large-scale water tank for seasonal thermal storage applications. *Energ Build* 2023;278:112620.
- [24] Steen D, Stadler M, Cardoso G, Groissböck M, DeForest N, Marnay C. Modeling of thermal storage systems in MILP distributed energy resource models. *Appl Energy* 2015;137:782–92.
- [25] Mukherjee U, Walker S, Marouf mashat A, Fowler M, Elkamel A. Development of a pricing mechanism for valuing ancillary, transportation and environmental services offered by a power to gas energy system. *Energy*. 2017;128:447–62.
- [26] Wu J, Lu Z, Qiao Y, Ynag H. Optimal operation of wind farm with hybrid storage devices considering efficiency characteristics of dynamic charging and discharging. *Automat Electric Power Syst* 2018;42. 41–7+101.
- [27] Ren F, Wei Z, Zhai X. A review on the integration and optimization of distributed energy systems. *Renew Sust Energ Rev* 2022;162:112440.
- [28] Sun L, You F. Machine learning and data-driven techniques for the control of smart power generation systems: an uncertainty handling perspective. *Engineering*. 2021;7.
- [29] Zhang Y, Hua QS, Sun L, Liu Q. Life cycle optimization of renewable energy systems configuration with hybrid battery/hydrogen storage: a comparative study. *J Energy Stor* 2020;30:101470.
- [30] Lyden A, Brown CS, Kolo I, Falcone G, Friedrich D. Seasonal thermal energy storage in smart energy systems: district-level applications and modelling approaches. *Renew Sust Energ Rev* 2022;167:112760.
- [31] Wang Y, Liu C, Qin Y, Wang Y, Dong H, Ma Z, et al. Synergistic planning of an integrated energy system containing hydrogen storage with the coupled use of electric-thermal energy. *Int J Hydrg Energy* 2023;48:15154–78.
- [32] Petkov I, Gabrielli P. Power-to-hydrogen as seasonal energy storage: an uncertainty analysis for optimal design of low-carbon multi-energy systems. *Appl Energy* 2020;274:115197.
- [33] Sánchez A, Martín M, Zhang Q. Optimal design of sustainable power-to-fuels supply chains for seasonal energy storage. *Energy*. 2021;234:121300.
- [34] Pu Y, Li Q, Zou X, Li R, Li L, Chen W, et al. Optimal sizing for an integrated energy system considering degradation and seasonal hydrogen storage. *Appl Energy* 2021;302:117542.

- [35] Gabrielli P, Acquilino A, Siri S, Bracco S, Sansavini G, Mazzotti M. Optimization of low-carbon multi-energy systems with seasonal geothermal energy storage: the Anergy grid of ETH Zurich. *Energy Conv Manag X* 2020;8:100052.
- [36] Chen X, Qiu R, Wu X. Multi-timescale capacity configuration optimization of energy storage equipment in power plant-carbon capture system. *Appl Therm Eng* 2023;227:120371.
- [37] Weimann L, Gazzani M. A novel time discretization method for solving complex multi-energy system design and operation problems with high penetration of renewable energy. *Comput Chem Eng* 2022;163:107816.
- [38] Gabrielli P, Gazzani M, Martelli E, Mazzotti M. Optimal design of multi-energy systems with seasonal storage. *Appl Energy* 2018;219:408–24.
- [39] Kotzur L, Markewitz P, Robinius M, Stolten D. Time series aggregation for energy system design: Modeling seasonal storage. *Appl Energy* 2018;213:123–35.
- [40] Dong H, Wu Y, Zhou J, Chen W. Optimal selection for wind power coupled hydrogen energy storage from a risk perspective, considering the participation of multi-stakeholder. *J Clean Prod* 2022;356:131853.
- [41] Dong H. Research code and data of 'Refined modeling and co-optimization of electric-hydrogen-thermal-gas integrated energy system with hybrid energy Storage'. https://github.com/SuperBean-Dong/paper_EHTG-IES; 2023.
- [42] Amr AA-R, AAM Hassan, Abdel-Salam M, El-Sayed AM. Enhancement of photovoltaic system performance via passive cooling: theory versus experiment. *Renew Energy* 2019;140:88–103.
- [43] Qin Y, Liu P, Li Z. Multi-timescale hierarchical scheduling of an integrated energy system considering system inertia. *Renew Sust Energ Rev* 2022;169:112911.
- [44] Mann RF, Amphlett JC, Hooper MAJ, Jensen HM, Peppley BA, Roberge PR. Development and application of a generalised steady-state electrochemical model for a PEM fuel cell. *J Power Sources* 2000;86:173–80.
- [45] Chen X, Gong G, Wan Z, Luo L, Wan J. Performance analysis of 5 kW PEMFC-based residential micro-CCHP with absorption chiller. *Int J Hydrol Energy* 2015;40:10647–57.
- [46] Khan MJ, Iqbal MT. Modelling and analysis of electro-chemical, thermal, and reactant flow dynamics for a PEM fuel cell system. *Fuel Cells* 2005;5:463–75.
- [47] Amores E, Rodríguez J, Carreras C. Influence of operation parameters in the modeling of alkaline water electrolyzers for hydrogen production. *Int J Hydrol Energy* 2014;39:13063–78.
- [48] Shen X, Zhang X, Li G, Lie TT, Hong L. Experimental study on the external electrical thermal and dynamic power characteristics of alkaline water electrolyzer. *Int J Energy Res* 2018;42:3244–57.
- [49] Sánchez M, Amores E, Rodríguez L, Clemente-Jul C. Semi-empirical model and experimental validation for the performance evaluation of a 15 kW alkaline water electrolyzer. *Int J Hydrol Energy* 2018;43:20332–45.
- [50] Janssen H, Bringmann JC, Emonts B, Schroeder V. Safety-related studies on hydrogen production in high-pressure electrolyzers. *Int J Hydrol Energy* 2004;29:759–70.
- [51] Ma Y, Wang H, Hong F, Yang J, Chen Z, Cui H, et al. Modeling and optimization of combined heat and power with power-to-gas and carbon capture system in integrated energy system. *Energy*. 2021;236:121392.
- [52] Jiang B, Zhang X. Experimental study on charging and discharging properties of LiFePO₄ batteries for electric vehicles. *Chinese J Power Sources* 2018;42: 494–6+571.
- [53] Bahl B, Kümpel A, Seele H, Lampe M, Bardow A. Time-series aggregation for synthesis problems by bounding error in the objective function. *Energy*. 2017;135:900–12.
- [54] Gabrel V, Lacroix M, Murat C, Remli N. Robust location transportation problems under uncertain demands. *Discret Appl Math* 2014;164:100–11.
- [55] Schlauchberger DP, Brown T, Schäfer M, Schramm S, Greiner M. Cost optimal scenarios of a future highly renewable European electricity system: exploring the influence of weather data, cost parameters and policy constraints. *Energy*. 2018;163:100–14.
- [56] Andrews J, Shabani B. Dimensionless analysis of the global techno-economic feasibility of solar-hydrogen systems for constant year-round power supply. *Int J Hydrol Energy* 2012;37:6–18.